JCB Journal of Cell Biology

ARTICLE

Assembly of γ-secretase occurs through stable dimers after exit from the endoplasmic reticulum

Rosanne Wouters[1,2*], Christine Michiels[1,2*], Ragna Sannerud[1,2*], Bertrand Kleizen[3], Katleen Dillen[1,2], Wendy Vermeire[1,2], Abril Escamilla Ayala[4], David Demedts[1,2], Randy Schekman[5], and Wim Annaert[1,2]

γ-Secretase affects many physiological processes through targeting >100 substrates; malfunctioning links γ-secretase to cancer and Alzheimer's disease. The spatiotemporal regulation of its stoichiometric assembly remains unresolved. Fractionation, biochemical assays, and imaging support prior formation of stable dimers in the ER, which, after ER exit, assemble into full complexes. In vitro ER budding shows that none of the subunits is required for the exit of others. However, knockout of any subunit leads to the accumulation of incomplete subcomplexes in COPII vesicles. Mutating a DPE motif in presenilin 1 (PSEN1) abrogates ER exit of PSEN1 and PEN-2 but not nicastrin. We explain this by the preferential sorting of PSEN1 and nicastrin through Sec24A and Sec24C/D, respectively, arguing against full assembly before ER exit. Thus, dimeric subcomplexes aided by Sec24 paralog selectivity support a stepwise assembly of γ-secretase, controlling final levels in post-Golgi compartments.

Introduction

γ-Secretase constitutes a di-aspartyl protease that cleaves type I transmembrane proteins within their membrane-spanning domain (De Strooper et al., 1998; Edbauer et al., 2003; Wolfe et al., 1999). This action requires a preceding shedding of the ectodomain to generate C-terminal fragments. The result of this dual processing is the release of a C-terminal intracellular domain into the cytosol and remaining short hydrophobic peptides into the extracellular milieu (De Strooper and Annaert, 2010; Escamilla-Ayala et al., 2020a). Currently, >100 substrates are identified, among which are the well-known amyloid precursor protein (APP) and Notch (Haapasalo and Kovacs, 2011; Jurisch-Yaksi et al., 2013). In the case of APP C-terminal fragment (CTF), γ-secretase processing releases short amyloid-β (Aβ) peptides of various lengths, of which those >42 aa are increasingly prone to aggregate (Jarrett et al., 1993). As such, they comprise the major components of senile plaques that, together with neurofibrillary tangles, are the chief neuropathological hallmarks of Alzheimer's disease (AD; Bancher et al., 1989; Iwatsubo et al., 1994). Because of its key role in Aβ production, γ-secretase remains a therapeutic target, although clinical trials targeting γ-secretase inhibition have failed thus far (De Strooper, 2014).

γ-Secretase is made up of four components: the catalytic subunit presenilin (PSEN), nicastrin (NCT), anterior pharynx-defective 1 (APH1), and presenilin enhancer 2 (PEN-2; Edbauer et al., 2003; Kimberly et al., 2003; Takasugi et al., 2003). The existence of two homologous PSENs (PSEN1 and PSEN2) and several APH1 isoforms generates separate complexes that have distinct subcellular distributions, providing a basis for substrate selectivity (Hébert et al., 2004; Sannerud et al., 2016; Shirotani et al., 2004). Mutations in the *PSEN* and *APP* genes cause early-onset familial AD (FAD) and increase total Aβ or the production of longer, more toxic Aβ peptides (Selkoe and Hardy, 2016; Szaruga et al., 2017). All four γ-secretase components are transmembrane proteins that are cotranslationally inserted in the ER; however, how assembly is regulated is still poorly understood.

The early biosynthetic pathway consists of three compartments: the ER, ER-Golgi intermediate compartment (ERGIC), and the Golgi apparatus. All three are critically involved in the proper assembly of multimeric protein complexes as part of secondary quality control mechanisms (Ellgaard and Helenius, 2003; Michelsen et al., 2005). Thus far, full γ-secretase assembly has been reported to take place in or during transport between pre-Golgi compartments (Capell et al., 2005; Kim et al., 2005; Kim et al., 2007; Kim et al., 2004), but the exact sequence of events and the essential compartments remain elusive. Moreover, none of the γ-secretase subunits bear confirmed ER exit or

[1]Laboratory for Membrane Trafficking, Vlaams Instituut voor Biotechnologie Center for Brain and Disease Research, Katholieke Universiteit Leuven, Leuven, Belgium; [2]Department of Neurosciences, Katholieke Universiteit Leuven, Leuven, Belgium; [3]Cellular Protein Chemistry, Bijvoet Center for Biomolecular Research, Faculty of Science, Utrecht University, Utrecht, The Netherlands; [4]Vlaams Instituut voor Biotechnologie BioImaging Core, Vlaams Instituut voor Biotechnologie Center for Brain and Disease Research, Leuven, Belgium; [5]Department of Molecular and Cell Biology and Howard Hughes Medical Institute, University of California, Berkeley, Berkeley, CA.

*R. Wouters, C. Michiels, and R. Sannerud contributed equally to this paper; Correspondence to Wim Annaert: wim.annaert@kuleuven.be.

retrieval motifs, arguing that additional mechanisms are at stake in directing assembly. For instance, retrieval of individual subunits, including NCT and PEN-2, is regulated through interaction with the Golgi-to-ER cargo retrieval receptor RER1p at the ERGIC/cis-Golgi (Kaether et al., 2007; Park et al., 2012; Spasic et al., 2007). This interaction negatively controls assembly, underscoring that affecting complex assembly in biosynthetic compartments impacts cellular γ-secretase activity. Other potential regulatory components of γ-secretase were identified, such as CD147 and TMP21, but their direct link to assembly has not been elucidated (Chen et al., 2006; Zhou et al., 2005).

ER exit is governed through cargo sorting into coat protein complex II (COPII)–coated vesicles (Lee et al., 2004). Herein, the small GTPase Sar1p is recruited to its ER-localized GTP exchange factor, Sec12p (Barlowe and Schekman, 1993; Sato et al., 1996). This initiates the sequential recruitment of COPII coat proteins, first the Sec23/24p complex and next the Sec13/31p complex, deforming the ER membrane along with packaging cargo into nascent vesicles (Barlowe et al., 1994; McCaughey and Stephens, 2019). Sec24p has four paralogs, and the presence of multiple cargo binding sites makes it an important player in capturing a broad range of cargo molecules exiting the ER (Mancias and Goldberg, 2008; Zanetti et al., 2012). Thus far, PSEN1 has been shown to largely depend on Sec24A for ER exit (Kim et al., 2007), and its packaging into COPII vesicles appeared to be uncoupled from APP (Kim et al., 2005), suggesting distinct carriers for export of enzyme and substrate. To our knowledge, no other transport motifs or mechanisms used by individual γ-secretase components to mediate ER-Golgi transport have been identified.

In this study, we combined cell fractionation and biochemical ER exit/COPII budding assays with blue native PAGE (BN-PAGE) and high-resolution imaging to uncover γ-secretase assembly in early biosynthetic compartments. Our data show that none of the individual subunits is required for the recruitment of other subunits in COPII vesicles but that individual subunits may prefer distinct COPII coat compositions for exit. We provide evidence that final assembly primarily occurs beyond the ER through a prior assembly of PSEN1/PEN-2 and NCT/APH1A dimers in the ER.

Results

Individual γ-secretase subunits can exit the ER independently from other subunits

Transport from the ER to the ERGIC/cis-Golgi is largely governed by the regulated sorting of cargo through COPII-coated transport carriers. As the transient nature of COPII vesicles complicates their analysis, we exploited an in vitro ER vesicle budding assay using semi-intact cells (SICs) to inspect the ER export regulation of individual γ-secretase subunits (Kim et al., 2007).

Following incubation of SICs with nucleotides and concentrated cytosol as a source of COPII proteins, newly formed COPII vesicles were separated from SICs by low-speed centrifugation, after which the budded vesicles were sedimented by ultracentrifugation. Omitting nucleotides or cytosol, or including dominant-negative Sar1b-H79G, blocks ER budding and was used for background subtraction and to demonstrate COPII selectivity, respectively (Fig. 1 A; Kim et al., 2007). Furthermore, the ER-resident protein ribophorin and the ER exit marker ERGIC53/p58 were included as negative and positive controls, respectively (Fig. 1 A, top panels). We first asked whether any of the γ-secretase subunits were required for the export of others by using WT and different knockout (KO) cell lines, including PSEN double-KO (PSEN-dKO), NCT-KO, APH1 triple-KO (APH1-tKO), and PEN-2-KO mouse embryonic fibroblasts (MEFs). As shown in Fig. 1 A and quantified in Fig. 1 B, p58 but not ribophorin was recovered in COPII vesicle fractions (budding reaction). Addition of recombinant Sar1b H79G fully blocked budding, underscoring that we selectively monitored COPII-dependent ER export. In WT SICs, all the individual γ-secretase subunits exited the ER in an Sar1p-dependent manner. Note that for PSEN1 and NCT, only the full-length (FL) and immature forms, respectively, were efficiently packaged in COPII vesicles, as shown previously in PSEN1-overexpressing cells (Kim et al., 2007). An important step in assembly of functional γ-secretase is the endoproteolysis of FL PSEN1 into an N-terminal fragment (NTF) and CTF. As PSEN1 endoproteolysis is strongly impaired or absent when other subunits are knocked out, FL PSEN1 accumulated and was increasingly recovered in COPII vesicles budding from NCT-KO, APH-tKO, and PEN-2-KO SICs (Fig. 1 A).

Overall, these data demonstrated that none of the γ-secretase components required the presence of all other subunits to become sorted into COPII vesicles, underscoring that full assembly of the γ-secretase complex is not a requirement for ER export. We noted also that, compared with p58/ERGIC53, the overall budding efficiency of γ-secretase subunits remained low, irrespective of the genotype. Of note, SICs derived from primary cortical neurons and glial cells gave similar results, underscoring comparable in vitro ER exit regulation in these specialized cell types (Fig. S1 A). Unfortunately, KO of each of the different γ-secretase subunits results in early embryonal lethality, preventing the generation of primary neurons. Therefore, experiments were performed on immortalized MEFs derived from these KO genotypes.

Subcellular distribution of mature γ-secretase complexes

We next explored the assembly state in the secretory pathway using complementary ultracentrifugation strategies to obtain enriched fractions of ER, ERGIC, early and late endosomes/lysosomes (next called "endosomal fraction"), and plasma membrane (PM; Figs. 2 A and S1). Subsequent extraction of organellar fractions using 0.5% *n*-dodecyl β-D-maltoside (DDM) and analysis by BN-PAGE allowed us to compare the relative enrichments for mature tetrameric complexes versus subcomplexes, as shown in Fig. 2, A and B (Fraering et al., 2004a; Kim et al., 2007; Spasic et al., 2007). In WT cells, NCT-APH1A dimers were clearly detected in ER fractions, but, compared with the full 440 kD complexes, they were strongly decreased in ERGIC fractions and were essentially absent in endosomal fractions (Fig. 2 A). Mature complexes, on the other hand, were poorly detected in the ER but markedly increased in the ERGIC and were the sole complexes observed in endosomal fractions (Fig. 2 A) and purified PMs (Fig. 2 B). We noticed that endosomal

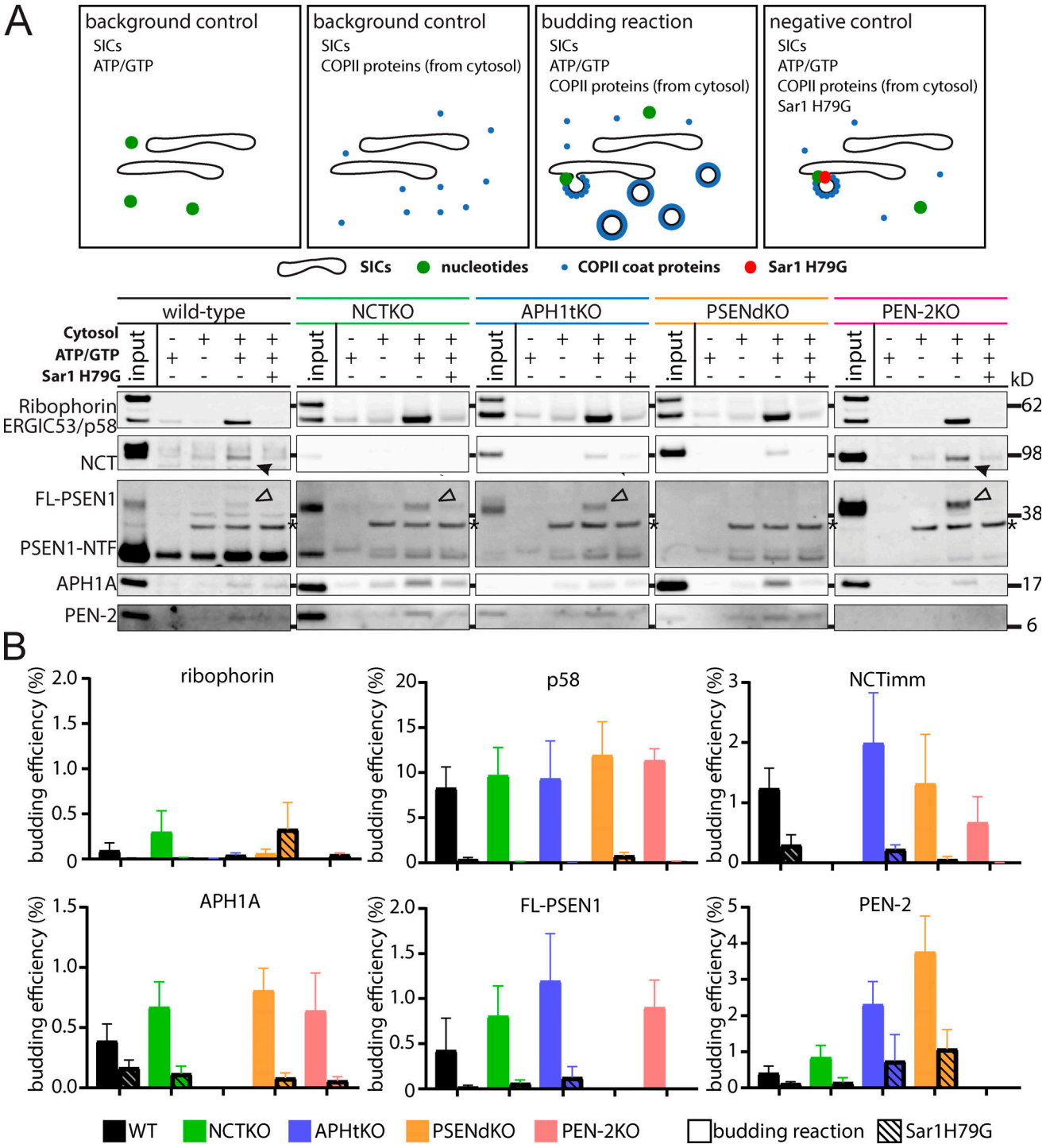

Figure 1. **ER exit of individual γ-secretase subunits does not require expression of all subunits.** SDS-PAGE of in vitro COPII vesicles from WT, PSEN-dKO, NCT-KO, and APH1-tKO SICs: 4.2% of SICs (input) and 100% of COPII vesicles were analyzed. Reactions without nucleotides (ATP + GTP) or cytosol were used for background subtraction. COPII budding was inhibited by mutant Sar1b H79G. **(A)** Scheme of assay and Western blot of COPII packaging using antibodies against ERGIC53/p58 (positive control), ribophorin (negative control), and γ-secretase subunits. Asterisks indicate an unrelated band as detected with anti-PSEN1 antibodies in PSEN-dKO fractions. In the different SICs, except PSEN-dKO, only PSEN1 FL exited the ER in an Sar1-dependent manner (open arrowheads). Except for their respective KO SICs, both APH1A and PEN-2 were recovered in COPII vesicles next to immature NCT (NCTimm; filled arrowheads). **(B)** Quantification of COPII budding efficiencies as the ratio of signal intensity of the input fraction to the COPII vesicle fraction, corrected for the background obtained in the absence of nucleotides. Graphs show mean budding efficiency ± SEM of at least three or four independent assays.

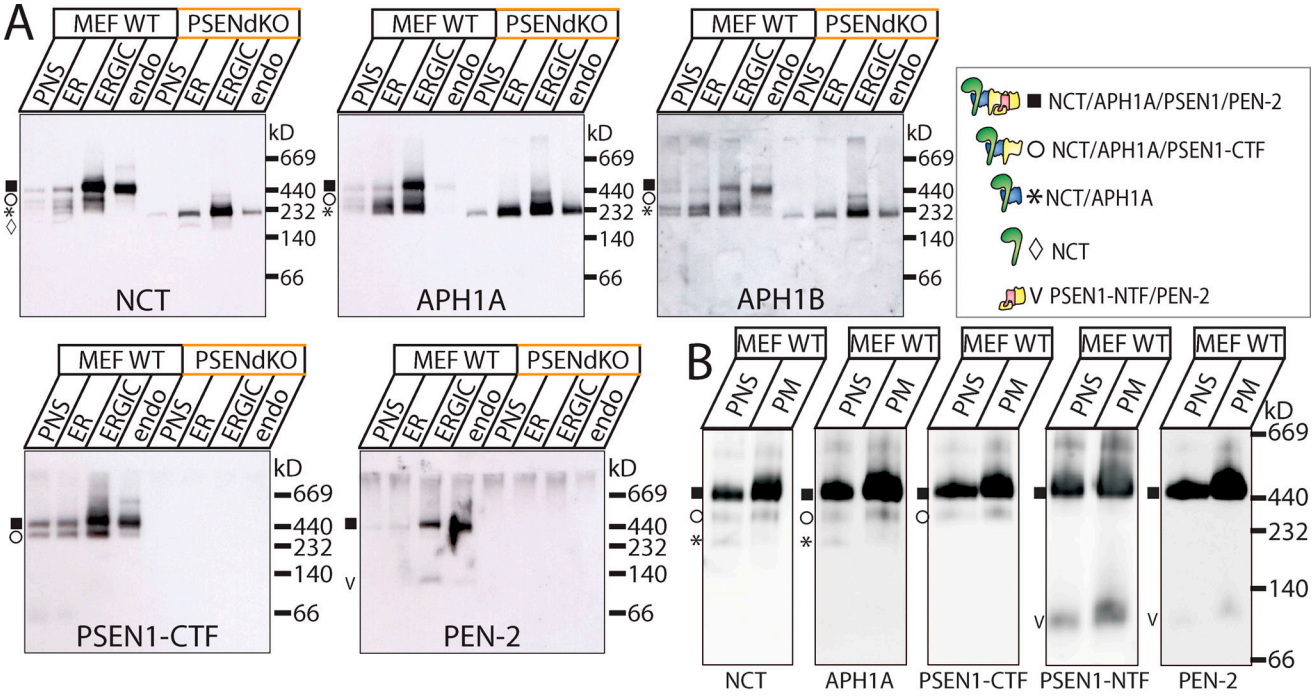

Figure 2. **γ-Secretase complexes enrich from ERGIC to endosomal fractions and PM (see also Fig. S1). (A)** BN-PAGE of γ-secretase complexes in PNS compared with enriched compartments (ER, ERGIC, and early to late endosomes/lysosomes [endo]) from MEF WT and PSEN-dKO (see Fig. S1). Membranes were extracted in 0.5% DDM to resolve complexes (Fraering et al., 2004a; Spasic et al., 2007), and equal protein amounts were loaded. Western blot for NCT, APH1A$_L$, PSEN1-CTF, and PEN-2 showed a gradual increase in the ratio of the 440 kD band (full complex; filled squares) versus ∼220 kD NCT/APH1A subcomplexes (asterisks), particularly between the ER and the ERGIC. Mature complexes were predominant in endosomal fractions. In PSEN-dKO, only NCT/APH1A subcomplexes were found in the ER and were most strongly enriched in the ERGIC. APH1B-containing complexes dominated in endosomal fractions. **(B)** BN-PAGE of DDM extracts of PNS and isolated PMs (Tharkeshwar et al., 2017). Only ∼440 kD full complexes (filled squares) were found positive for all subunits, including APH1A, being highly abundant at the cell surface. Open circles indicate the NCT/APH1A/PSEN1-CTF subcomplex. Representative Western blots are shown.

fractions were devoid of APH1A; instead, APH1B was strongly enriched, indicating that this differently composed complex was more enriched in endosomes, whereas APH1A complexes were more abundant at the cell surface (Fig. 2 B). In MEF PSEN-dKO cells, immature NCT-APH1A subcomplexes accumulated in enriched ER and ERGIC fractions, whereas their presence sharply declined in endosomal fractions (Fig. 2 A). This indicates that in the absence of PSEN expression, the dimeric NCT-APH1 subcomplex was retained in early biosynthetic compartments. Dimeric subcomplex retention was further supported in studies using confocal microscopy, wherein we analyzed the distribution of GFP-PSEN1 stably rescued in PSEN-dKO MEFs (mimicking the WT situation with GFP-PSEN1–containing full complexes) as well as in PSEN-dKO/NCT-KO and PSEN-dKO/PEN-2-KO MEFs (preventing full assembly and GFP-PSEN1 endoproteolysis). Of note, the N-terminal GFP tag did not affect the functionality of PSEN1 in γ-secretase (Fig. S2 A) or its localization (Escamilla-Ayala et al., 2020b; Sannerud et al., 2016). In the presence of all four subunits, GFP-PSEN1 colocalized with markers for post-Golgi compartments, including LAMP1 and with transferrin receptor (TfR; Fig. 3 A, top panel). In contrast, in an NCT- or PEN-2-KO background, GFP-PSEN1 predominantly colocalized with mCherry-Sec61B, indicating ER retention (Fig. 3 A, middle and bottom panels). We could not colocalize GFP-PSEN1 with p58 in ERGIC compartments (Fig. 3 B), in agreement with the low ER budding efficiencies observed in our in vitro assay (Fig. 1 B).

We argued next that blocking ER exit would result in a more marked entrapment of subunits in p58-positive ER exit sites (ERESs). To test this, we treated cells with a mixture of nocodazole (Noco) and brefeldin A (BFA) because this has been shown to confine secretory cargo in ERES through uncoupling cargo sorting from later transport (Dukhovny et al., 2008). This treatment results in a conversion of the tubulovesicular ERES to more globular membranes that accumulate cargo while excluding ER-resident proteins. Quantitative confocal analysis revealed a moderate but significant increase of GFP-PSEN1 in p58-positive ERES in NCT-KO and PEN-2-KO cells compared with WT, in accordance with our in vitro budding data (Fig. 3 C and Fig. 1 B). Super-resolution visualization further confirmed the presence of GFP-PSEN1 in or near enlarged ERES (Fig. 3 D). We next blocked COPI-mediated retrograde transport using transiently overexpressed HA-tagged Arf1-Q71L in GFP-PSEN1–rescued PSEN-dKO, PSEN-dKO/NCT-KO, and PSEN-dKO/PEN-2-KO MEFs. Whereas p58/ERGIC-53 immunoreactivity, as expected, strongly accumulated in Arf1-Q71L–positive compartments, no concomitant accumulation of GFP-PSEN1 in either NCT or PEN-2-KO conditions was observed, arguing against active recycling of unassembled subunits/subcomplexes (Fig. 3 E). Of note, in NCT-KO and PEN-2-KO backgrounds, GFP-PSEN1 was confined in

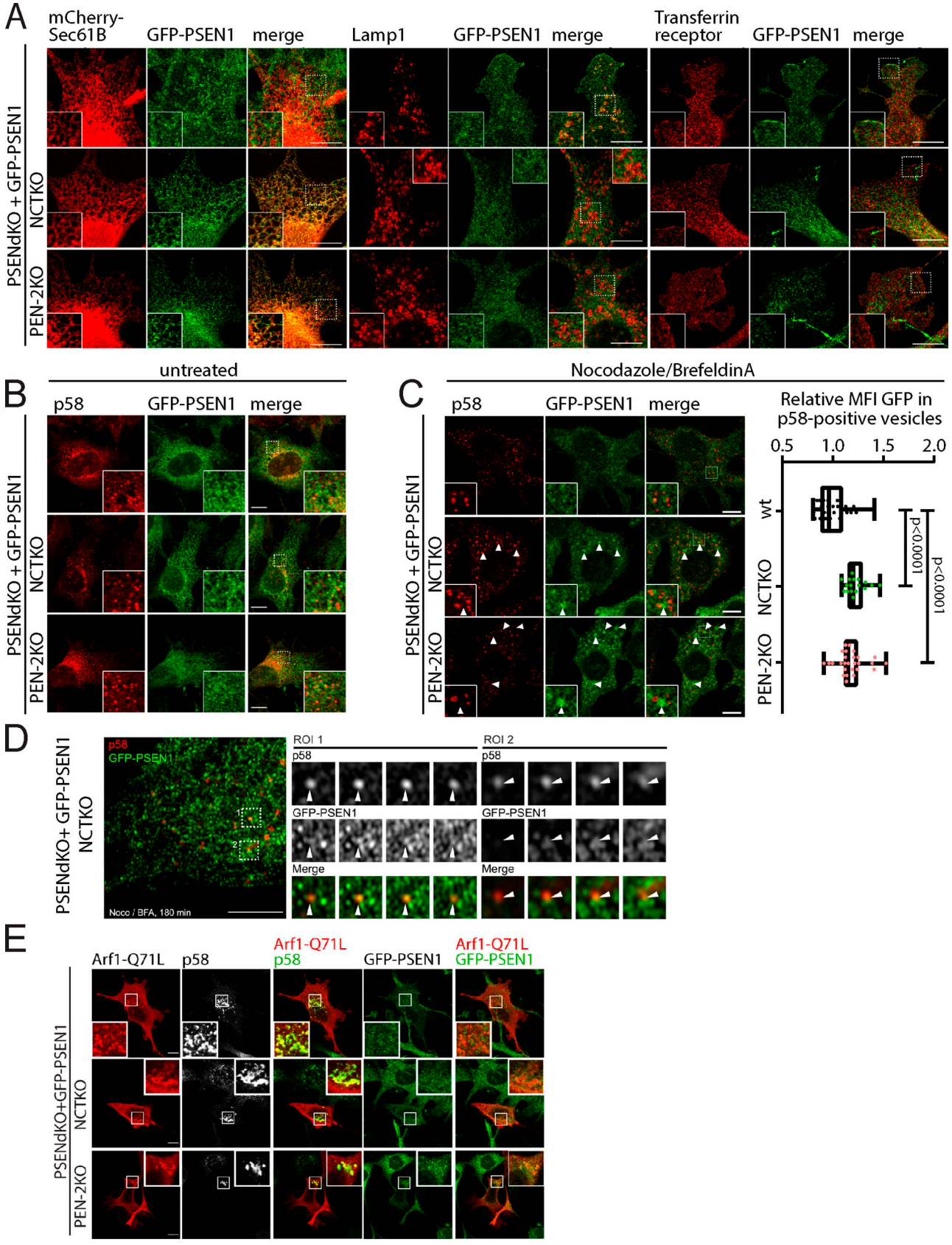

Figure 3. **γ-Secretase subunits are present in minute amounts in p58-positive structures. (A and B)** GFP-PSEN1 was retained in the ER in the absence of NCT or PEN-2. MEFs expressing GFP-PSEN1/γ-secretase (top, mimicking WT situation), lacking NCT (middle) or PEN-2 (bottom), were transfected with mCherry-SEC61B to visualize the ER. After 24 h, fixed cells were stained for Lamp1 or TfR (A) or p58 (B). When γ-secretase complex formation was restored,

GFP-PSEN1 codistributed on Lamp1-positive organelles and at the cell surface (marked by TfR in A). p58 and GFP-PSEN1 colocalized in none of the conditions (B). Insets: Zooms of the squares on the merged panels. **(C)** Localization of GFP-PSEN1 in Noco/BFA-induced dilated ERES. PSEN1/PSEN2/NCT-tKO MEFs stably rescued with GFP-PSEN1 treated with 1 µg/ml Noco on ice (20 min) followed by 1 µg/ml Noco + 5 µg/ml BFA (37°C, 3 h), were fixed and immunostained for GFP (green) and p58 (red, identifying dilated ERES). Arrowheads: GFP-PSEN1 accumulation close to enlarged ERES. Right: Quantification of mean fluorescence intensity (MFI) of GFP in p58-positive enlarged structures showed increased colocalization of GFP-PSEN1 with p58 in NCT-KO and PEN-2-KO. The box and whisker graph shows all the data points. P values were determined by unpaired Student's t-test. **(D)** Airyscan imaging of NCT-KO MEFs treated as in C. Left: Merge of GFP (green) and p58 (red) with two regions of interest (ROIs 1 and 2). Middle and right: Zooms of ROIs as Z-stack images (0.2-µm steps), correlating frame-by-frame GFP-PSEN1 presence in p58-positive dilated ERES (arrowheads). **(E)** GFP-PSEN1 does not accumulate upon Arf1Q71L expression. MEFs expressing GFP-PSEN1/γ-secretase (top) or lacking PEN-2 (middle) or NCT (bottom) were transfected with HA-Arf1Q71L. After 24 h, cells were fixed and stained for GFP, HA, and p58. p58, but not GFP-PSEN1, is strongly enriched in Arf1-Q71L–positive compartments. Scale bar = 10 µm (A–C and E); 5 µm (D).

clear patches, often in the neighborhood of enlarged ERES (Fig. 3 C, arrowhead), indicating that, aside from the small amounts exiting the ER in a COPII-dependent manner, major amounts of GFP-PSEN1 are retained in specific ER regions or domains. We next explored whether, in a given γ-secretase subunit KO background, remaining subunits exit the ER independently or associated in subcomplexes.

γ-Secretase subcomplexes preferentially exit the ER in de novo COPII transport carriers

It is believed that γ-secretase assembly starts with the formation of an NCT-APH1A subcomplex with which PSEN1 and PEN-2 then associate (Fraering et al., 2004a; LaVoie et al., 2003). Alternatively, assembly might occur through the association of two preformed dimeric subcomplexes of NCT/APH1 and PSEN1/PEN-2 (Spasic and Annaert, 2008). To determine the γ-secretase assembly status in relation to ER export, we inquired to what extent subcomplexes are preferentially sorted in COPII vesicles, using the in vitro ER budding/COPII reconstitution assay. For this analysis, we extracted the input and COPII vesicle fractions with 0.5% DDM to discriminate between mature complexes and subcomplexes of γ-secretase (see above and Fraering et al., 2004a). To increase the detection limit for BN-PAGE, we scaled up the budding reaction threefold.

For WT SICs, BN-PAGE analysis clearly revealed that only endogenous monomeric NCT and minute levels of dimeric NCT/APH1A exited the ER in an Sar1/COPII-dependent manner (Fig. 4 A, indicated by open diamonds and asterisks, respectively; compare lanes 2 and 3). Larger complexes, such as the NCT/APH1A/PSEN1-CTF (Fig. 4 A, open circle) subcomplex and fully assembled γ-secretase (Fig. 4 A, filled square), were also present in these fractions; however, for these species, in vitro budding was not blocked by the dominant-negative Sar1 H79G (Fig. 4 A; compare lanes 2 and 3 of each blot). Thus, the larger complexes were not packaged into COPII vesicles but were possibly derived from other unrelated vesicular budding events. Note that the trimeric NCT/APH1A/PSEN1-CTF subcomplexes might also represent full complexes that have lost the PSEN1-NTF and PEN-2 during extraction (Fraering et al., 2004a; Kim et al., 2007). Of note, similar results were obtained in SICs derived from primary rat glial cells (Fig. S3 A).

We next analyzed 0.5% DDM-extracted budding reactions obtained from the different KO MEFs and compared the ER exit of monomers and subcomplexes with WT MEFs, using herein anti-NCT as a reference (left panels in Fig. 4, A–C). COPII vesicles budding from NCT-KO SICs packaged a dimeric PSEN1/PEN-2 complex (Fig. 4 B). Here, PSEN1 represented the FL protein because this band was detected by both anti–PSEN1-NTF and -CTF antibodies and migrated at a lower mobility than the PSEN1-NTF/PEN-2 band (this latter band came from membranes other than COPII vesicles because its detection was not Sar1 dependent). In APH1-tKO SICs, the same FL-PSEN1/PEN-2 dimers were recovered in addition to a prominent band representing monomeric NCT, suggesting that they too exited the ER independently. To test this further, we analyzed PSEN-dKO SICs (Fig. 4 C). Indeed, again, NCT and APH1A were packaged in COPII vesicles predominantly as dimers, with only trace amounts of monomeric NCT. Interestingly, COPII vesicles produced from PEN-2-KO SICs accumulated mainly the trimeric NCT/APH1/FL-PSEN1 complexes with much lower amounts of NCT/APH1 dimers and monomeric NCT. Whereas in the absence of PEN-2 expression, PSEN1 does not become endoproteolysed (Prokop et al., 2004), it now appeared not to require PEN-2 for binding the NCT/APH1A, resulting in the formation of trimeric complexes that exit the ER. Furthermore, from the results in both PSEN-dKO and PEN-2-KO SICs, we concluded that FL PSEN1 binds directly to NCT/APH1A and not via PEN-2. This was confirmed by coimmunoprecipitation using anti-NCT mAb 9C3, demonstrating that in WT extracts, all four subunits were recovered in the bound fractions (Fig. S3 B). On the other hand, in APH1-tKO, PSEN-dKO, and PEN-2-KO extracts, only the cognate partner subunit identified by BN-PAGE was coimmunoprecipitated with immature NCT, validating the use of BN-PAGE in combination with DDM extraction for analyzing complex formation during ER exit.

Thus, our results are not in favor of full complexes being formed before ER exit. Instead, the findings support the idea that mainly two dimer subcomplexes, NCT/APH1 and PSEN1/PEN-2, are formed in the ER and become independently packaged in COPII transport vesicles. In this result, the PSEN1/PEN-2 complexes comprise FL PSEN1, in agreement with the idea that PSEN1 endoproteolysis occurs beyond the ER (Kim et al., 2007). Because our data underscored the preformation of dimers as a step before full assembly, we wondered about the physiological relevance of this particular sequence of events. We considered the possibility that dimerization might promote subunit stability and thereby reduce premature degradation by the ER-associated degradation pathway. To test this, we explored the stability of all subunits in the different KO backgrounds using cycloheximide (CHX) treatment over 6- and 24-h periods (Fig. 5 A). Immature NCT steady-state levels were lowered in the absence of APH1, whereas this was not the case in PSEN- or PEN-2-KO

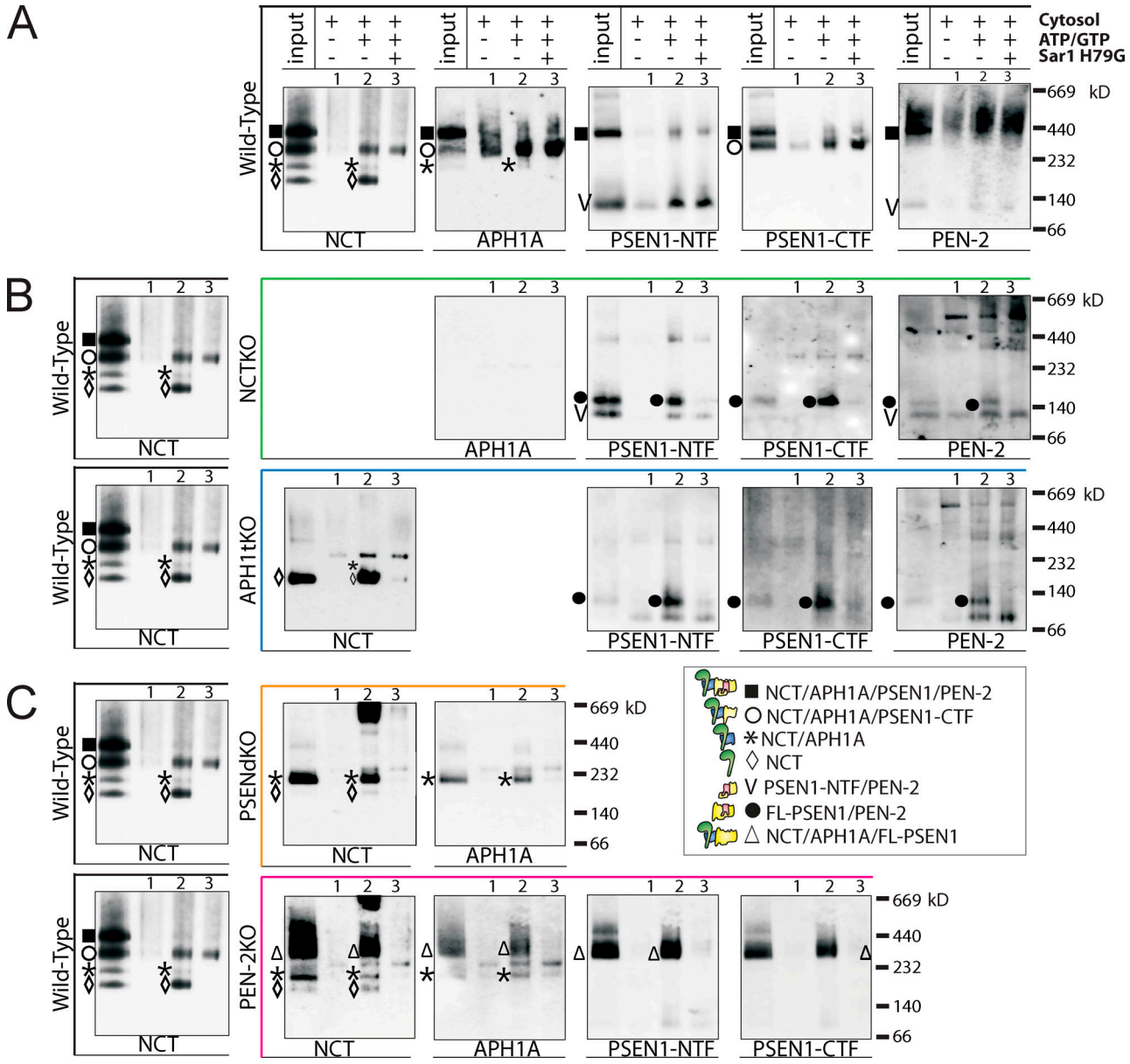

Figure 4. **Deficiency of a given γ-secretase component allows ER exit of remaining subunits in subcomplexes. (A)** BN-PAGE of γ-secretase in 0.5% DDM-extracted COPII vesicles of WT, **(B)** NCT-KO and APH1-tKO, and **(C)** PSEN-dKO and PEN-2-KO SICs. Budding reactions without cytosol or nucleotides or with Sar1-H79G were for background subtraction and specificity, respectively. Antibodies against γ-secretase subunits identified monomers and subcomplexes (Fraering et al., 2004b). Full complexes did not exit the ER Sar1 dependently (compare lanes 2 and 3), whereas KO SICs efficiently packaged preceding monomers/subcomplexes (dimeric NCT/APH1 [asterisks] in PSEN-dKO, FL PSEN1/PEN-2 [filled circles] in NCT-KO and APH1-tKO; NCT/APH1A/FL-PSEN1 [open triangles] in PEN-2-KO; lane 2 in all blots) in an Sar1-dependent manner. Lane 1, without ATP/GTP = negative control.

backgrounds (Fig. 5 A, bar graphs). Likewise, APH1A levels were clearly decreased in the case of NCT-KO but maintained in the other KO backgrounds, consistent with a mutual stabilizing effect on NCT-APH1 dimers. Similarly, PSEN deficiency substantially affected PEN-2 stability (Fig. 5 A, bar graphs). The stabilizing features of dimers appear to be limited in time as well. In NCT-KO and APH1-tKO MEFs, FL PSEN1 and PEN-2 ultimately were degraded after extended CHX treatment (Fig. 5 A, line graphs), as observed as well for NCT and APH1A in the case of PSEN deficiency. The outlier appeared to be PEN-2-KO MEFs: here, FL PSEN1 was dramatically increased and remained stable even after 24-h CHX treatment (Fig. 5 A), likely due to its incorporation into stable NCT/APH1A/FL-PSEN1 trimers, the predominant subcomplex seen in the ER budding assays as well (Fig. 4 C). Notably, the formation of dimers before full assembly remains visible in the molecular structure of γ-secretase, where the NCT/APH1A dimer is clearly distinguishable from the PSEN1/PEN-2 dimer (Fig. 5 B and Video 1; Yang et al., 2021). Whereas each dimer features intimate stacking between the respective transmembrane domains (TMDs), both dimers appear to align next to each other, leaving a noticeable gap and supporting an assembly from dimers (dashed lines in Fig. 5 B).

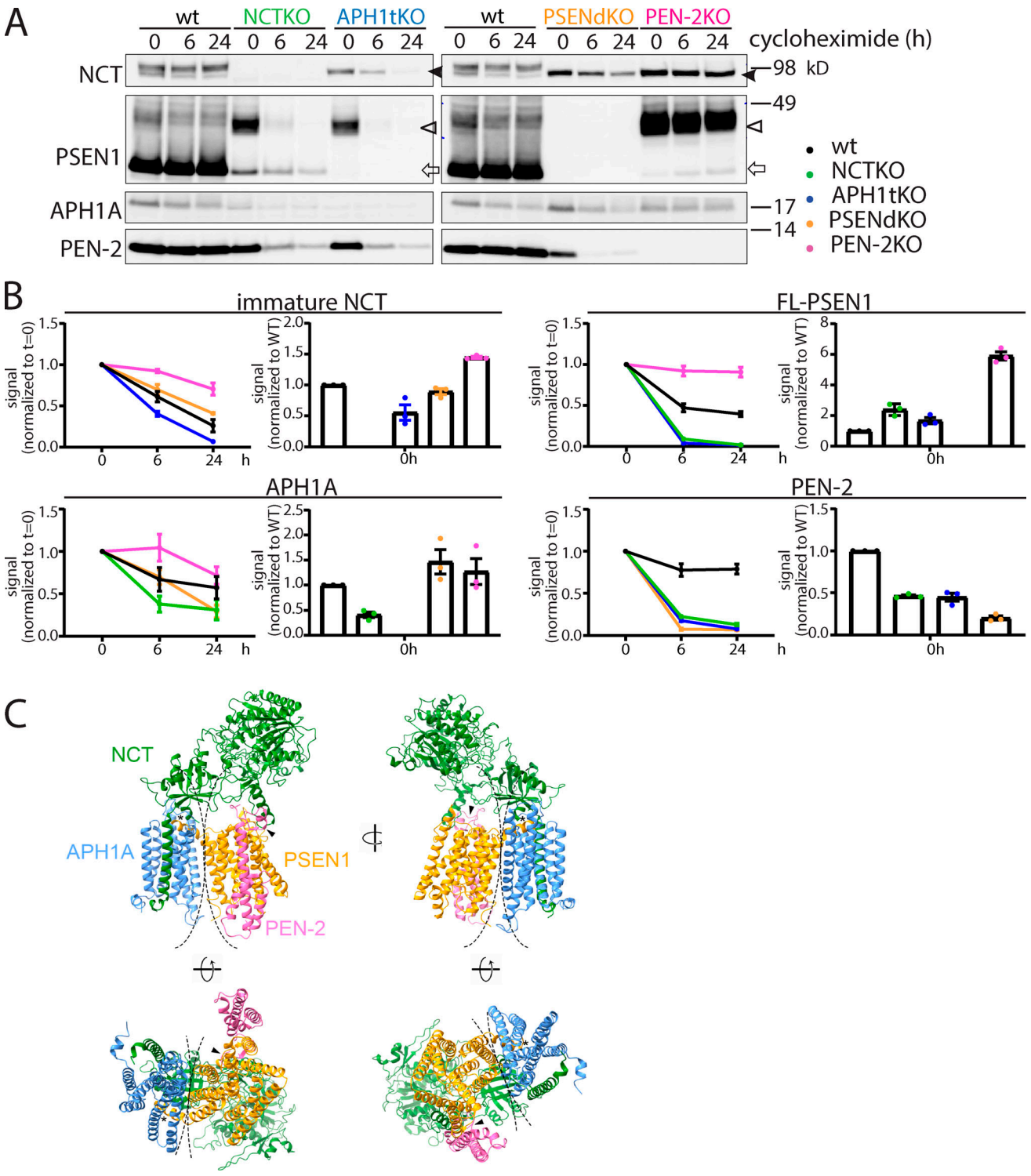

Figure 5. **Dimer formation stabilizes monomeric subunits, maintaining a steady ER resource for assembly of γ-secretase complexes. (A)** SDS-PAGE of subunit steady-state levels and degradation after CHX treatment in MEF WT, NCT-KO, APH1-tKO, PSEN-dKO, and PEN-2-KO. Representative blots after 0-h (steady state), 6-h, or 24-h CHX treatment (filled arrowheads: immature NCT; open arrowheads: FL PSEN1; open arrows: PSEN1-NTF). **(B)** Quantification for degradation normalized to 0 h and for steady-state levels to WT levels (0 h). Immature NCT degraded fastest and had the lowest steady-state levels in the absence of APH1 and vice versa. Likewise, PEN-2 degraded fastest and had the lowest steady-state levels in the absence of PSEN. FL PSEN1 degraded slowest and was most stable in the absence of PEN-2 (i.e., when NCT/APH1A/PSEN1 trimer formation was observed). Graphs show mean normalized protein levels ± SEM (n = 3) **(C)** Lateral (top) and bottom (bottom) views of the γ-secretase structure (Protein Data Bank accession no. 6LR4, prepared using UCSF Chimera; Pettersen et al., 2004) with NCT (green), APH1A (blue), PSEN1 (orange), and PEN-2 (pink). Asterisks indicate the connection between the PSEN1 C-terminus and APH1A; arrowheads indicate PSEN1–PEN-2 interaction; dotted lines indicate the space between dimers (Video 1).

PSEN1/PEN-2 is essentially connected to APH1A through the C-terminus of PSEN1 (asterisk in Fig. 5 B). The dimer pairing may be further stabilized or strengthened through the large NCT ectodomain that bends over the PSEN1/PEN-2 dimer.

γ-Secretase subunits may use distinct COPII coat compositions to exit the ER

Except in the case of PEN-2-KO MEFs, mostly dimeric subcomplexes exit the ER. A potential mechanism to keep dimers separated during ER exit could be through Sec24 isoform specificity. To test this, we adapted our budding assay by reducing cytosol concentrations to levels that do not support COPII vesicle budding and adding recombinant COPII coat proteins.

The COPII coat is formed on the ER membrane from three subunits: Sar1-GTP and the dimeric Sec23/24 and Sec13/31 coat proteins (Fig. 6 A; Bickford et al., 2004; Fath et al., 2007; Zanetti et al., 2012). Sec24 is the major cargo selection subunit of the COPII coat that binds ER exit motifs (Adolf et al., 2016; Miller et al., 2002; Miller et al., 2003; Miller et al., 2005). In humans, there are four Sec24 isoforms (A–D) and two Sec23 isoforms (A and B), creating versatility of ER cargo selection. To explore the COPII coat preference for the different γ-secretase subunits, we expressed and purified the different Sec24 isoforms, each in a complex with Sec23A (Kim et al., 2007; Mancias and Goldberg, 2008), and combined these with recombinant Sar1 and Sec13/31 to reconstitute COPII vesicle budding. Of note, because the Sec23A/Sec24B subcomplex is highly proteolytically sensitive, this isoform was excluded. Besides ERGIC53/p58, we included a second control, RER1p, a Golgi-to-ER cargo receptor (Annaert and Kaether, 2020). Assay conditions including nucleotides and cytosol were used to normalize ER export efficiencies by the different Sec24 isoforms. Lowering cytosol concentration reduced COPII packaging activity to basal levels (Fig. 6 A; quantified in Fig. 6 B), which could be marginally restored by adding recombinant Sec13/31 or Sar1 (Fig. 6). When Sec23A/24 isoforms were additionally included, efficient isoform-specific packaging was observed (Fig. 6). Whereas all isoforms supported COPII-dependent exit of the control cargo proteins ERGIC53/p58 and RER1p, the packaging efficiencies for Sec24C and Sec24D were significantly higher. The preference of RER1p for Sec24C/D is in accordance with a recent proteome analysis of COPII vesicles (Adolf et al., 2019). In MEF WT cells, Sec24C/D isoforms mainly supported COPII sorting of immature NCT, similar to that seen for RER1p, whereas FL PSEN1 preferred the Sec24A isoform for packaging (Fig. 6, A and B, top panel; and as reported in Kim et al., 2007). In APH-tKO, the same preference of NCT for Sec24C/D and PSEN1 for Sec24A was found (Fig. 6, A and B, middle panels). Surprisingly, in the absence of PEN-2, this specificity was lost because both NCT and PSEN1 were recovered in vesicles with all three Sec24 isoforms in PEN-2-KO cells (Fig. 6, A and B, bottom panels). This agreed with the sorting of the trimeric NCT/APH1A/PSEN1 subcomplex in COPII vesicles of PEN-2-KO cells we detected earlier (Fig. 4 C, bottom). This trimer now may combine the cargo sorting information in one complex, resulting in a loss of Sec24A isoform specificity.

To further determine the source of this apparent Sec24 isoform preference, we took advantage of a FAD-associated PSEN1 mutation, PSEN1ΔE9, that is largely deficient in incorporation into COPII-coated vesicles (Kim et al., 2007). Exon 9 skipping in these FAD patients causes a 29-aa deletion in the PSEN1 sequence, removing the endoproteolytic cleavage site and a conserved diacidic DXE motif (Fig. 7 A), that is reported to sort ER cargo into COPII vesicles (Mancias and Goldberg, 2008; Nishimura et al., 1999). To determine if the DXE motif in PSEN1 is involved in ER export, we translated PSEN1-DXE mutants in vitro in SICs followed by the COPII-dependent ER export assay. The advantage of this approach is that we followed the ER export of only newly synthesized and radiolabeled FL PSEN1 (Kim et al., 2007). Removing the charged residues of the DXE motif, or even reversing the sequence of two negative charges (EXD), showed identical reduction in ER export compared with the PSEN1ΔE9 mutant (Fig. S3, C–E). Clearly, loss of exon 9 removes not only the endoproteolytic cleavage site but also a conserved ER export motif (Fig. S3, C–E; and Fig. 7 A), explaining the strong reduction in ER exit of this FAD mutation.

Mutating the DXE motif provided an opportunity to investigate COPII-dependent export of PSEN1 in relation to the ER exit of the dimeric PSEN1/PEN-2 and NCT/APH1 subcomplexes. We therefore stably reintroduced WT-PSEN1 and mutant PSEN1-APA [mutating Asp (D) and Glu (E) residues in the DPE motif to Ala (A)] into PSEN-dKO using retroviral transduction (Fig. S3 F; Sannerud et al., 2016). ERGIC53/p58 sorting into COPII vesicles was not different between both cell lines, indicating comparable ER exit efficiencies (Fig. 7, B and C). Sar1-dependent ER export of PSEN1-APA was almost reduced to background levels when compared with the presence of Sar1b H79G, mimicking the effect of the PSEN1ΔE9 FAD mutant (Kim et al., 2007) and our results shown in Fig. S3, C–E. Importantly, the reduced ER export of PSEN1 was paralleled by an almost equal decline in ER export of endogenous PEN-2, underscoring that PSEN1 and PEN-2 jointly exit the ER. These data are consistent with the formation of a PSEN1/PEN-2 subcomplex before or during ER exit. However, because PEN-2 can still be detected in COPII vesicles in the absence of PSEN1 (Fig. 1), the association of PEN-2 with PSEN1 is not an absolute requirement for PEN-2 to become sorted in COPII vesicles. In contrast, ER exit of immature NCT was unaffected in the presence of the PSEN1-APA export mutant (Fig. 7, B and C). This could be explained by different COPII coat preferences for ER exit of the NCT/APH1 dimer versus the PSEN1/PEN-2 dimer. Because no obvious ER export motif could be found in NCT, we wondered whether a specific domain in NCT is responsible for the Sec24C/D preference. We generated NCT-KO MEFs stably rescued with different deletion mutants wherein either the ectodomain or the intracellular domain was deleted or wherein the TMDs of NCT and of the neuronal cell adhesion protein Telencephalin (TLN; also called ICAM-5) were swapped (Fig. S4, A and B). All of these NCT variants were capable of exiting the ER in de novo COPII vesicles, demonstrating that the nature of the preference is unlikely to be caused through a direct interaction of NCT with Sec24C/D (Fig. S4 C). In conclusion, our data are consistent with a spatial separation of the NCT/APH1A and PSEN1/PEN-2 dimers during ER exit, to which differential Sec24 isoform specificity may partially contribute.

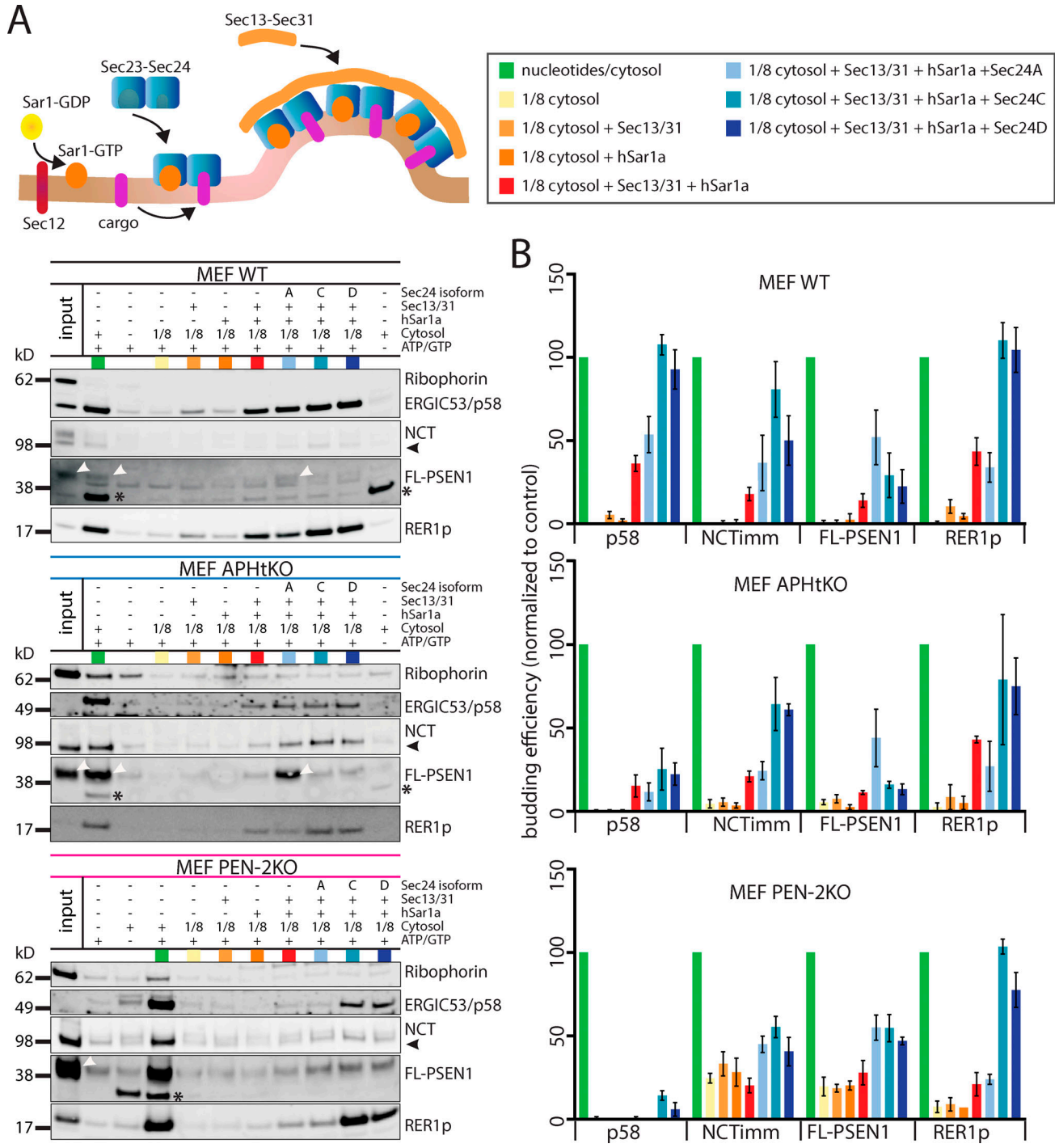

Figure 6. **PSEN1/PEN-2 and NCT/APH1A dimers preferentially exit the ER through distinct Sec24 paralog requirements. (A)** Scheme of COPII budding. Representative Western blot of COPII vesicles with different efficiencies of Sec24 isoforms A, C, and D in packaging NCT and FL PSEN1 in MEF WT, APH-tKO, and PEN-2-KO SICs. Ribophorin was a negative control, and ERGIC-53/p58 and RER1p were positive controls (filled arrowheads: immature NCT; white arrowheads: FL PSEN1; asterisks: aspecific band). **(B)** Quantification of A. NCT was preferentially sorted through Sec24C/D isoforms, whereas FL PSEN1 favored the Sec24A isoform. Data are presented as mean ± SEM (n = 3 or 4). NCTimm, immature NCT.

Discussion

In this study, we combined cell fractionation and in vitro reconstitution of COPII carrier formation in distinct γ-secretase subunit KO backgrounds to conclude that, in WT cells, heterodimeric NCT/APH1A and PSEN1/PEN-2 subcomplexes preferentially exit the ER in a COPII-dependent manner to become fully assembled shortly thereafter, likely in the transition of uncoated transport vesicles to the ERGIC (Fig. 7 C). This is corroborated by our findings that (1) KO of a given subunit results in the increased appearance of monomers and dimers in COPII vesicles; (2) PSEN1 and NCT prefer different Sec24 isoforms in COPII vesicle packaging; and (3) inhibiting PSEN1 packaging in

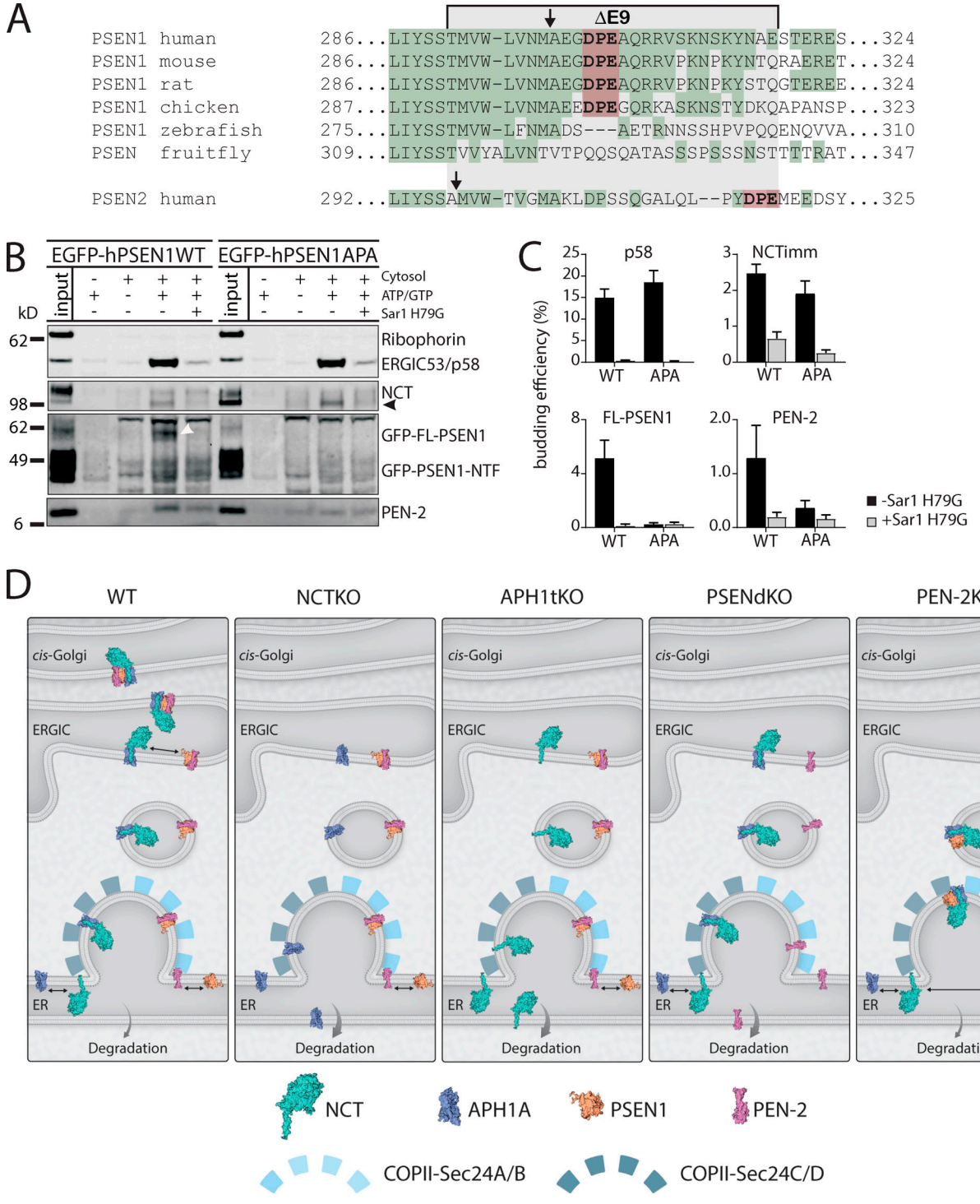

Figure 7. **Deficiency in ER exit of PSEN1 affects PEN-2 but not NCT packaging in COPII vesicles. (A)** Sequence alignment of the deleted sequence in FAD PSEN1ΔE9. Bold red: COPII binding motif DPE. Green: Identical residues. The motif is highly conserved in mammals and birds but absent in lower vertebrates (fish) and fly. **(B)** Representative Western blot of COPII vesicles in PSEN-dKO MEFs stably rescued with EGFP-PSEN1WT or EGFP-PSEN1APA using antibodies against NCT, GFP (GFP-FL-PSEN1, white arrowhead; and GFP-PSEN1-NTF), and PEN-2. Filled arrowheads: Immature NCT (NCTimm) packaged in COPII vesicles. ERGIC53/p58: Positive control blocked by mutant Sar1 H79G. **(C)** Quantification of B. Mutating DPE to APA affected COPII packaging of FL PSEN1 and PEN-2 but not NCT. Mean ± SEM; $n = 6$. **(D)** Buckle-up model for γ-secretase assembly. Monomer subunits and dimers exit the ER with NCT/APH1 and PSEN1/PEN-2 preferring Sec24C/D and Sec24A, respectively. In WT cells, NCT/APH1A and PSEN1/PEN-2 dimers are preformed in the ER and buckle up in a full complex after ER exit, likely during ERES-to-ERGIC transition. Prior dimer formation may prevent premature degradation of monomeric subunits, but the exact mechanisms of how they are sorted into COPII vesicles versus retained in the ER remain to be investigated. Assembly to a full complex may hide known/unknown interaction motifs, allowing the complex to exit the early biosynthetic compartments to post-Golgi compartments. In KO backgrounds, and due to a failed assembly, preceding dimers (in NCT, APH1, PSEN1-KO) and trimers (PEN-2-KO) are increasingly recovered in COPII vesicles. Assembled monomers may be routed to degradation (generated by Somersault 18:24; https://www.somersault1824.com/).

COPII carriers, through mutation of a DPE sorting motif, blocks ER exit of PEN-2 but not that of NCT. Prior dimer formation may be a way to protect unassembled subunits from premature degradation. Monomeric subunits appeared to be more rapidly degraded overall (Fig. 5 B).

Interestingly, the dimer assembly signature remains visible in the high-resolution structure of γ-secretase, suggesting a "buckle-up model" for dimer assembly (Fig. 5 B). We propose that, upon arrival in the COPII-devoid ERES or ERGIC, both dimers partner. Herein the large ectodomain of NCT (the "belt") associates with PSEN1 and PEN-2 through mostly van der Waals contacts between an α-helix with surrounding loops in NCT and the first hydrophilic loop domain of PSEN1 and the C-terminal end of PEN-2 (Bai et al., 2015; Petit et al., 2019). At the center of the horseshoe shape of γ-secretase, PSEN1 binds to APH1 through a "buckle" shaped by three C-terminal residues of PSEN1 that click into a hydrophobic pocket formed by TMD2/3/4/6/7 of APH1A, providing a firmer connection (Bai et al., 2015).

In the absence of full complex assembly (i.e., when any of the four subunits is knocked out), subcomplexes accumulate in nascent COPII transport carriers. This might suggest that, when not incorporated in full complexes, subcomplexes are actively recycled from the Golgi to the ER. However, we could not find experimental support for this. First, only very small amounts of escaped subunits/subcomplexes were recovered in COPII vesicles. Second, in an NCT-KO background, microscopy showed abundant ER localization of GFP-PSEN1 and virtually no detectable levels in p58-positive ERGIC. Minute amounts of GFP-PSEN1 could be found in or near p58-positive ERES only when ER exit was blocked. Likewise, ARF1-Q71L–mediated blockade of retrograde Golgi-to-ER transport did not result in an accumulation of GFP-PSEN1 in cis-Golgi. Thus, active recycling of immature subunits is likely not part of the quality control mechanism regulating complex assembly, as suggested previously (Spasic et al., 2007; Sannerud and Annaert, 2009). The longer residence of major pools of immature subunits or subcomplexes in the ER underscores the existence of additional, yet unknown, mechanisms, preventing premature assembly as well as efficiently sorting subunits or dimers toward COPII-coated exit sites. Such retention or crowding seems to occur in ER domains proximal to ERES locations (Fig. 3, C and D). The accumulation of subcomplexes in nascent COPII transport carriers in each KO background, at the expense of their monomeric status (most obvious for NCT), indicates that full assembly on its own is not rate limiting for ER exit; rather, it underscores that separate subcomplexes first exit the ER before assembly occurs.

Previous reports provided evidence for ER-localized γ-secretase assembly (Capell et al., 2005; Holmes et al., 2014; Kim et al., 2004). Yet, in most of these reports, NCT was modified with an ER retrieval motif. This may activate the retrieval of complexes assembled in the ERGIC/cis-Golgi, explaining the observed pool of active γ-secretase in the ER. Kim et al. (2007) also used the cell-free COPII vesicle formation reaction and concluded that full complexes, though inactive, can exit the ER. However, these authors used digitonin instead of DDM for BN-PAGE analysis. Digitonin extraction results in a major band of ∼440 kD, as shown previously (Fraering et al., 2004a). Although Kim et al. (2007) showed that the release of vesicles containing this species was nucleotide dependent, we found it not to be Sar1p dependent and thus not a COPII-mediated process (Fig. S5). The 440 kD band is more prominent in digitonin than in DDM extraction, pointing to a higher instability of the complex in the latter case. This instability might be related to the PSEN1-NTF–CTF interaction because, for WT SICS, a similar Sar1p independency was observed for the trimeric NCT/APH1/PSEN1-CTF and PSEN1-NTF/PEN-2 subcomplexes (Fig. 4).

We further show that NCT and FL PSEN1 (i.e., a component of each respective dimer) have a different Sec24 isoform preference. Although this suggests dimer-specific cargo sorting, it does not imply that the dimers are sorted via distinct COPII-mediated ERES and thus transport carriers. Instead, Sec24 paralogs may form combinatorial COPII coats, expanding the range of cargo being packaged in COPII carriers (Shimoni et al., 2000). Whereas we find a Sec24A/B binding motif in PSEN1 but not in the other dimer, other mechanisms besides the Sec24 isoform preference must be involved to keep the NCT/APH1A and PSEN1/PEN-2 heterodimers spatially separated during cargo sorting and ER exit (Fig. 7 C). Notably, this Sec24 preference is lost in PEN-2-KO cells, where PSEN1 is joined by NCT and APH1A in one trimeric subcomplex. Thus, PEN-2 might prevent premature γ-secretase assembly in the ER, providing the cell with an elegant mechanism that avoids premature processing of (immature) substrates. However, additional experiments are needed to scrutinize this. How dimers finally assemble is not yet known, but a possible scenario could be that this occurs from the moment the COPII coats dissociate from the nascent transport carrier and thus very shortly after ER exit. This agrees with a strong increase in mature γ-secretase complexes in enriched ERGIC fractions (Fig. 2 A).

The DXE motif identified in the cytosolic loop domain of PSEN1 is a recognition site for Sec24A/B (Mancias and Goldberg, 2008; Miller et al., 2002; Miller et al., 2003; Mossessova et al., 2003; Nishimura et al., 1999), explaining its preference for Sec24A in ER exit (Kim et al., 2007). However, this defect in ER exit is kinetic in nature because the PSEN1-APA mutant eventually reaches post-Golgi compartments, such as the cell surface (Fig. S3 G), reminiscent of what was observed for the PSEN1ΔE9 mutant (Kim et al., 2007). How may PSEN1 overcome this delay in ER export when no (known) export motifs are found in PEN-2? One possibility is through other proteins that associate in the ER with PSEN1. For instance, the SNARE protein Sec22b was identified as a PSEN1-interacting protein (Wakabayashi et al., 2009). Sec22b selectively binds Sec24A/B as well, and this binding is conserved from yeast to humans (Mancias and Goldberg, 2007; Miller et al., 2003). It is thus conceivable that in the absence of a functional DPE motif, PSEN1 benefits from the interaction with Sec22b to exit the ER.

Sec24C/D selectivity in COPII packaging is mediated through IxM motifs in cargo proteins (Mancias and Goldberg, 2008); however, no such motif was found in NCT or APH1. A deletion strategy did not identify a domain in the topology of NCT required for ER exit (Fig. S4 C). As described above, an interaction with other cargo molecules, such as RER1p, may provide sorting information (Spasic et al., 2007). A recent proteomics profiling

of purified COPII transport carriers also revealed a preference of RER1p, though not fully penetrant, for Sec24C/D isoforms (Adolf et al., 2019), suggesting it might coexit the ER with NCT as well, instead of playing a role only in Golgi-to-ER retrieval. An alternative explanation could be the recently reported cargo crowding as a novel mechanism to regulate bulk flow of proteins out of the ER (Gomez-Navarro et al., 2020).

A possible consequence of the stepwise assembly through dimers after ER exit could be a quality control mechanism that prevents premature formation of this protease complex in an early biosynthetic compartment. Because all γ-secretase substrate precursors are translocated in the ER and undergo folding before COPII-mediated exit, such a mechanism could prevent the untimely processing of substrates (i.e., before they actually execute their function in mostly post-Golgi compartments). In addition, differences in translation, translocation, and/or folding as part of the ER primary quality control may generate non-stoichiometric levels of the different subunits: dimer formation before ER exit may restore such imbalance and safeguard stoichiometric exit of the four subunits while simultaneously preventing full complex assembly in the ER. If the subcomplexes are separated by Sec24 paralogs within the same COPII vesicle, following ER exit, the disassembly of the COPII coat may facilitate the encountering of the heterodimers, leading to full assembly. Alternatively, if the subcomplexes are sorted into distinct COPII vesicles, coat disassembly combined with homotypic fusion events would lead to the same outcome. This event may sterically mask hitherto exposed retention/retrieval motifs in the ERGIC/cis-Golgi, allowing the full complex to progress through the Golgi for further maturation. The assembly status is thus coupled to forward transport in a quality control process resembling "hide and run" (Michelsen et al., 2005). This process referred originally to Arg-based ER motifs in polytopic membrane proteins that are part of functional heteromultimeric complexes, including, for instance, the ATP-sensitive K^+ channel (Zerangue et al., 1999), γ-aminobutyric acid B receptor (Margeta-Mitrovic et al., 2000), and glutamate receptors (Scott et al., 2003; Xia et al., 2001). Given the broad range of substrates and associated pathways controlled by γ-secretase, tuning and regulating its assembly after ER exit but before entrance into the Golgi provides a spatiotemporal mechanism to regulate overall intramembrane proteolysis by γ-secretase. Consequently, aberrant complex assembly may have a significant impact on many physiological and pathological processes (Jurisch-Yaksi et al., 2013).

Materials and methods

Cell culture

Studies were performed in WT MEFs, MEFs deficient for PSEN1 and PSEN2 (PSEN-dKO; Nyabi et al., 2003), for all three rodent APH1 variants (APH1-tKO; Serneels et al., 2005), for NCT (NCT-KO; provided by P. Wong, The Johns Hopkins University School of Medicine, Baltimore, MD; Li et al., 2003), and for PEN-2 (PEN-2-KO; Bammens et al., 2011). Pulse-chase experiments (related to Fig. S3, C–E) were performed in Neuro2a cells. All cell lines were routinely maintained in DMEM/F-12 (Life Technologies) supplemented with 10% FCS (Gibco) and in a humidified chamber with 5% CO_2 at 37°C.

Cortical neuron cultures were prepared from embryonic day 17–18 fetal mice according to (Banker and Goslin, 1998). Single-cell suspensions obtained from the cortex of individual embryos were plated on poly-L-lysine–coated plastic dishes (Nunc) in MEM supplemented with 10% horse serum. After 3–4 h, culture medium was replaced by serum-free neurobasal medium with B27 supplement (Gibco BRL). Cytosine arabinoside (5 mM) was added 24 h after plating to prevent nonneuronal (glial) cell proliferation. Cortical neurons on plastic dishes were used at day 7 after plating. Glial cultures were prepared from postnatal day 1 rat pups according to Goslin and Banker (1991). Single-cell suspensions obtained from the cortex of individual embryos were plated in a T75 flask in MEM (Life Technologies) supplemented with 10% FCS (Gibco). The next day, cells were shaken vigorously and washed with HBSS-Hepes (Gibco) to remove contaminating cells; this was repeated after 3 d. Glial cells were used after 7 d.

Antibodies

The following pAbs were purchased: rabbit anti-Rab11 (Life Technologies), rabbit anti-PSEN1 (ab24748; Abcam), rabbit anti–PEN-2 (ab18189; Abcam), rabbit anti–early endosome antigen 1 (sc-33585; Santa Cruz Biotechnology), chicken anti-GFP (GFP-1010; Aves), and rabbit anti-NCT (5665; Cell Signaling Technology). The following mAbs were commercially obtained: rat anti-LAMP1 (sc-19992; Santa Cruz Biotechnology), mouse anti-LAMP1 (BD Biosciences), mouse anti-TfR (clone H68.4; Life Technologies), mouse anti-Aβ against aa 4–10 (WO2; Sigma-Aldrich), and mouse anti–coat protein D subunit (sc-514104; Santa Cruz Biotechnology). Other antibodies were generously provided: mAb to Rab5 (R. Jahn, Max Planck Institute for Biophysical Chemistry, Göttingen, Germany), pAb against Rab7 (P. Chavrier, Centre National de la Recherche Scientifique, Paris, France), pAbs against ribophorin and ERGIC53/p58 (Schekman laboratory), and pAb against cathepsin D (P. Saftig, Institut of Biochemistry, Kiel, Germany). Rabbit pAb against APP C-terminus (B63.3), PSEN1-NTF (B19.3), PEN-2 (B126.1), APH1A (B80.3), and telencephalin (TLN; B36.1) and mAbs against NCT (9C3) and PEN-2 (mAb 7D3) were generated in-house (Annaert et al., 1999; Esselens et al., 2004). The following secondary antibodies were used: goat anti-rabbit HRP (1706515; Bio-Rad Laboratories), goat anti-mouse HRP (1706516; Bio-Rad Laboratories), rabbit anti-goat HRP (P044901; Agilent), goat anti-chicken Alexa Fluor 488 (A32931; Thermo Fisher Scientific), goat anti-mouse Alexa Fluor 568 (A11031; Thermo Fisher Scientific), and goat anti-rabbit Alexa Fluor 555 (A21429; Thermo Fisher Scientific).

Expression vectors and generation of stable rescue cell lines

cDNAs encoding FL PSEN1 were cloned into plasmid murine stem cell virus (pMSCV) for retrovirus production. The DPE motif in PSEN1 was mutated to APA using the QuikChange II Site-Directed Mutagenesis Kit (Agilent Technologies) according to the manufacturer's instructions, with the forward and reverse primers being 5′-ATGGCAGAAGGAGCCCCGGCAGCTCAAAGG

AG-3′ and 5′-CTCCTTTGAGCTGCCGGGGCTCCTTCTGCCAT-3′, respectively. Virus was produced in HEK293T cells by cotransfecting pMSCV expressing the gene of interest with the helper plasmid pIk (Ecopac) using FuGENE6 (Promega) according to the manufacturers' instructions. For transduction, viral particles were diluted in medium containing polybrene (8 ng/µl; Sigma-Aldrich). Medium was refreshed after 24 h. To establish stable cell lines, we selected transduced cells using 5 µg/ml puromycin (Sigma-Aldrich).

Retroviral vectors encoding WT NCT and the different deletion mutants as well as mutants with swapped TMD domains and their respective stable rescue in NCT-KO MEFs have been generated and characterized previously (Spasic et al., 2007).

PSEN-dKO and PSEN1/PSEN2/NCT-tKO MEFs stably rescued with GFP-PSEN1 using the retroviral pMSCV vector were generated and validated previously (Escamilla-Ayala et al., 2020b; Sannerud et al., 2016). PEN-2 was knocked out in PSEN-dKO MEFs using CRISPR/Cas9 gene editing as described (Escamilla-Ayala et al., 2020b). Briefly, a target sequence was designed using the web-based CRISPR Design Tool (http://crispor.tefor.net/) to select the genomic sequence target in mouse *PEN2* (5′-CACCGAAGATAGTACTTCCGGCAC-3′). The selection marker puromycin of the pX459 vector (Addgene) was swapped to hygromycin. Oligo pairs (Integrated DNA Technologies) encoding guide sequences were annealed and ligated into the plasmid pX459hygro following the Zhang laboratory protocol (https://www.addgene.org/crispr/zhang/). PSEN-dKO MEFs rescued with GFP-PSEN1 were transfected with pX459hygro-PEN2 using FuGENE6 (Promega) or with pX459hygro (control). The following day, cells were selected with hygromycin (400 µg/ml) for 72 h. Surviving cells were grown to full confluency and passaged, and aliquots were frozen in liquid N_2 until use. KO of PEN-2 was confirmed by Western blotting.

Noco/BFA induced dilated ERES membranes (Dukhovny et al., 2008)

MEFs grown on coverslips were incubated on ice with 1 µg/ml Noco (SML1665; Sigma-Aldrich) for 20 min. To accumulate secretory cargo in ERESs, we shifted cells to 37°C for 3 h in the presence of 1 µg/ml and 5 µg/ml BFA (B5936; Sigma-Aldrich), after which they were fixed in 4% PFA and processed for immunofluorescence as described in Sannerud et al. (2016).

In vitro ER budding assay

Preparation of SICs

SICs were prepared as described (Wilson et al., 1995), starting from MEF cells grown to 80% confluency in three 10-cm-diameter dishes (~16.5 × 10^6 cells). After washing with $PBS^{-/-}$, cells were trypsinized by incubation at RT for 1–2 min with 1 ml warm (37°C) trypsin-EDTA (Invitrogen) per dish. Trypsinization was stopped by adding 100 µl 1 mg/ml Soybean Trypsin Inhibitor (Fluka) per dish. Cells were resuspended in 6 ml ice-cold KHM buffer (110 mM KOAc; 20 mM Hepes-NaOH, pH 7.2; 2 mM MgOAc) per dish and pooled in two 15-ml falcon tubes. All further steps were performed at 4°C. Cells were centrifuged (3 min, 1,000 g_{av}) and resuspended in 6 ml KHM buffer per tube. To permeabilize cells, we added 6 µl digitonin (40 mg/ml; Calbiochem) per Falcon tube, which was gently mixed, followed by incubation on ice for exactly 5 min. Permeabilization was stopped by adding 8 ml KHM buffer per Falcon tube followed by centrifugation (3 min, 1,000 g_{av} [average of minimal and maximal centrifugal force]). The pellets were resuspended in 1 ml KHM buffer, transferred to 1.7-ml low-retention tubes, and centrifuged for 15 s at 10,000 g_{av} in an Eppendorf centrifuge. SICs were resuspended in 400 µl KHM buffer per tube and pooled. The concentration of SICs was determined by mixing 20 µl SIC suspension with 980 µl KHM buffer and measuring OD_{600nm}. The volume of SICs needed for one budding reaction was calculated using the following formula: $x = 0.96/OD_{600nm}$.

In vitro ER budding assay

Each reaction was performed in a total volume of 300 µl in 1.7-ml low-retention tubes as described (Kim et al., 2005; Kim et al., 2007) with some modifications. First, appropriate amounts of SICs were added to the reaction mixture, containing (when indicated): (1) 30 µl 10× ATP regeneration mix (rATP; 10 mM ATP; Amersham), 500 µM GDP-mannose (Sigma-Aldrich), 400 mM phosphocreatine (Sigma-Aldrich), 2 mg/ml creatine phosphokinase (Sigma-Aldrich), pH 6.8, in buffer B88 containing 5 mM MgOAc or 30 µl buffer B88 (20 mM Hepes-NaOH, pH 7.2; 250 mM sorbitol; 150 mM KOAc; protease inhibitor [PI; EDTA-free]) containing 5 mM MgOAc; (2) 9 µl 10 mM GTP (Roche); (3) 1–1.5 mg rat liver cytosol or an equal volume of buffer E; or (4) 0.3–3 µg purified hamster Sar1b H79G. Reaction mixtures were adjusted to 300 µl with buffer B88. All reagents were mixed on ice. COPII vesicle formation was initiated by incubating the reaction mixture at 30°C for 45 min and terminated by transfer to 4°C. After centrifugation (25 min at 14,000 g_{av}) to separate COPII vesicles (supernatant S1) from SICs (input P1), S1 was ultracentrifuged (TLA-100/TLA-100.4 rotor; 30 min at 122,000 g_{av}) to sediment COPII vesicles (P2). Pellet P1 (input) and P2 were solubilized in NuPAGE sample buffer, and, respectively, 4.2% of the input fraction (P1) and 100% of the vesicle fraction (P2) were analyzed by SDS-PAGE and Western blotting.

Preparation of rat liver cytosol

Rat liver cytosol was prepared as described (Nohturfft et al., 2000). Following 24-h starvation, two young male rats (Sprague-Dawley or Wistar) were anesthetized, and their livers were perfused with 0.9% NaCl through the portal vein. Dissected livers were minced and weighed. All the next steps were performed at 4°C. Per gram of liver, 2 ml ice-cold buffer E (50 mM Hepes-NaOH, pH 7.2; 250 mM sorbitol; 70 mM KOAc; 5 mM K-EGTA; 0.5 mM MgOAc; PI) supplemented with 1 mM DTT was added, followed by homogenization by 10 strokes in a Potter-Elvehjem Teflon glass homogenizer. The total homogenate (TH) was centrifuged (1,000 *g* for 10 min); the supernatant was sequentially centrifuged at 26,900 g_{av} for 30 min using a JA-20 rotor and three times at 118,000 g_{av} for 1 h using a 70Ti rotor. The final supernatant was collected (omitting the fat layer on top), aliquoted, snap frozen in liquid nitrogen, and stored at −80°C until use.

Purification of human Sar1a and hamster Sar1b H79G (Kim et al., 2005)

Escherichia coli BL21 cells carrying the Sar1a or Sar1b H79G sequence fused to GST were grown at 37°C in 1 liter 2× YT (1.6%

Bacto tryptone, 1.0% Bacto yeast extract, 0.5% NaCl) supplemented with ampicillin (40 µg/ml) to an OD_{600nm} of 0.5, transferred to 30°C, and further grown to an OD_{600nm} of 1.0. Protein expression was induced with 0.1 mM IPTG (2 h, 30°C), and cells were harvested (25 min, 1,250 g_{av}). All the next steps were performed at 4°C. The pellet was resuspended in 25 ml of TBST (50 mM Tris-HCl, pH 7.4; 150 mM NaCl; 0.1% Tween-20; 10 µM GDP), then incubated with lysozyme (0.8 mg/ml, 20 min), after which Triton X-100 was added (1% final). Next, cells were sonicated (Branson; four pulses of 30 s, output control 6–7, duty cycle 50%) and successively centrifuged, first at 17,640 g_{av} (25 min) and next at 117,750 g_{av} (1 h), to remove cell debris. The supernatant was mixed with 2 ml TBST-washed glutathione Sepharose 4B beads (GE Healthcare; 1 h), after which they were centrifuged (1,500 g_{av}, 5 min), then washed four times with ice-cold TBST, once with TBS (50 mM Tris-HCl, pH 7.4; 150 mM NaCl; 10 µM GDP), and once with TCB (50 mM Tris-HCl, pH 8,0; 250 mM KOAc; 5 mM $CaCl_2$; 5 mM $MgCl_2$; 10 µM GDP). Beads were transferred to a column and incubated with 4 U thrombin (Roche Applied Science) in a final volume of 8 ml TCB (90 min at RT). The eluate containing human Sar1a or hamster Sar1b H79G cleaved off the GST fusion protein was collected and dialyzed against dialysis buffer (160 mM KOAc; 20 mM Hepes-NaOH, pH 6.8; 5 mM $MgCl_2$; 10 µM GDP; 5% glycerol; 5 mM β-mercaptoethanol) three times for 3 h each time. Finally, proteins were concentrated (Vivaspin, 100 kD cutoff; Sartorius), aliquoted, snap frozen in liquid N_2, and stored at −80°C.

Recombinant COPII coat proteins

Sf9 cells infected with either Sec23A/*His6*-Sec24 (isoforms A to D) or Sec13/*His6*-Sec31A viruses were harvested and sonicated in lysis buffer (20 mM Hepes, pH 8.0; 500 mM KOAc; 250 mM sorbitol; 10% glycerol; 10 mM imidazole; 0.1 mM EGTA; and 5 mM β-mercaptoethanol; supplemented with PI). Next, the lysate was centrifuged twice (as above). The cleared lysate was incubated with prewashed Ni-agarose resin (1 h, 4°C under slow rotation) and transferred to a column. After the column was first washed with lysis buffer and washing buffer (lysis buffer + 50 mM imidazole), recombinant protein complexes were eluted with elution buffer (lysis buffer + 250 mM imidazole). All the next steps were as for Sar1b purification (see above).

Cell fractionation

ER fractionation

The method of Hammond and Helenius (1994) was used with minor modifications. MEFs grown to 80–90% confluency (~150 × 10^6 cells/experiment) were washed, harvested in ice-cold Dulbecco's PBS, and centrifuged for 5 min at 4°C at 650 g_{av}. The pellet was resuspended in 1 ml homogenization buffer (10 mM triethanolamine; 10 mM acetic acid; 250 mM sucrose; 1 mM EDTA; 1 mM DTT, pH 7.4) and homogenized by 10 passages through a ball bearing cell cracker (clearance 10 µm; Isobiotex). PIs were added to the TH, followed by centrifugation for 10 min at 650 g_{av} at 4°C in an Eppendorf centrifuge. Postnuclear supernatant (PNS) was collected and loaded on top of a 10–24% Nycodenz gradient preformed on a cushion of 400 µl 27.6% Nycodenz stock (Axis-Shield) in 10 mM Tris (pH 7.4), 3 mM KCl, and 1 mM EDTA. The gradient was ultracentrifuged at 169,000 g_{av} for 1.45 h at 4°C in an SW41 rotor. 12 1-ml fractions were collected from the top of the gradient, and equal volumes of each fraction were analyzed by Western blotting.

Isolation of ERGIC compartments

Fractions enriched in ERGIC were obtained from MEFs as described (Annaert et al., 1999; Schweizer et al., 1991). MEFs were grown to 80–90% confluency (~450 × 10^6 cells/experiment), washed once with 0.9% NaCl and once with buffer A (250 mM sucrose; 10 mM triethanolamine HCl; pH 7.4), harvested in buffer B (250 mM sucrose; 1 mM Na_2 EDTA; 10 mM triethanolamine HCl; pH 7.4), and centrifuged for 5 min at 800 g_{av}. The cell pellet was resuspended in 5 ml buffer B and homogenized by 10 passages through a ball bearing cell cracker (clearance 10 µm). PIs were added to the TH, followed by centrifugation for 10 min at 800 g_{av} at 4°C in an Eppendorf centrifuge. PNS was collected and diluted to 30 ml with buffer B. After addition of 3.96 ml iso-osmotic Percoll, the mixture was centrifuged at 31,360 g_{av} for 41 min at 4°C in a JA-20 rotor, forming a self-generating Percoll gradient. After centrifugation, three opaque layers are visible: at the top, at approximately two-thirds of the gradient (starting from the bottom), and at the bottom of the gradient. Fractions (23) of 1.5 ml were collected from the top of the gradient. The fractions corresponding to the clear layer between the middle and bottom opaque layers (F10→F18) were pooled (pool) and adjusted to 30% Nycodenz by addition of 75% Nycodenz stock solution in buffer C (1 mM Na_2EDTA; 10 mM triethanolamine HCl; pH 6.5). Starting from three ultracentrifugation tubes, 6 ml of the mixture was loaded at the bottom of each tube. Three identical step gradients were formed by sequentially layering 3 ml each of 27% and 18.5% Nycodenz in buffer C, followed by buffer B up to the top. After ultracentrifugation (87,000 g_{av} for 19 h at 4°C in an SW41 rotor), the enriched ERGIC fraction was visible as an opaque band at the 18.5–27% interface, and a thinner opaque band was seen in the uppermost portion of the 18.5% Nycodenz cushion (I1). Both bands were collected separately and pooled for the three gradients, diluted with buffer C and centrifuged at 265,000 g_{av} for 1 h at 4°C in a 70Ti rotor. The pellets were resuspended in PBS, and equal amounts of protein were analyzed by Western blotting.

Enrichment of early and late endosomal fractions

The method of Gorvel et al. (1991) as modified by Sannerud et al. (2016) was used. MEFs were grown to 80–90% confluency (~250 × 10^6 cells/experiment), washed, and harvested in ice-cold Dulbecco's PBS. After centrifugation (5 min at 4°C at 650 g_{av}), the cell pellet was resuspended in homogenization buffer (250 mM sucrose; 3 mM imidazole; pH 7.4) and homogenized by four passages through a ball bearing cell cracker (clearance 10 µm). PIs were added to the homogenate, followed by centrifugation (10 min at 800 g_{av} and 4°C in an Eppendorf centrifuge). PNS was collected and adjusted to 40.6% sucrose using a stock solution of 62% sucrose, 3 mM imidazole (pH 7.4), and 1 mM EDTA, and 4 ml was loaded on the bottom of an ultracentrifugation

tube. A step gradient was formed by sequentially layering 3.7 ml 16% sucrose in D_2O (Sigma-Aldrich), 3 mM imidazole (pH 7.4), 0.5 mM EDTA, and 3.0 ml 10% sucrose in D_2O, 3 mM imidazole (pH 7.4), 0.5 mM EDTA, and 1.5 ml homogenization buffer on top of it. After ultracentrifugation (151,000 g_{av} for 1.40 h at 4°C in an SW41 rotor), 12 fractions were collected from the top of the gradient, and equal amounts of protein were analyzed by Western blotting. Late and early endosomal fractions were strongly enriched in fractions 2–5 (Sannerud et al., 2016).

Magnetic isolation of PMs

For the chemical synthesis and manufacturing of amino lipid–coated superparamagnetic iron oxide nanoparticles (SPIONs), we refer to Tharkeshwar et al. (2017) and Thimiri Govinda Raj et al. (2011).

Starting from four to six 10-cm dishes, WT and PSEN-dKO MEFs were grown to near confluency (90%). After placing on ice and washing with ice-cold DMEM (once) and PBS (three times), MEFs were incubated (20 min at 4°C) with amino lipid SPIONs diluted in PBS (2 mg/ml). Next, unbound amino lipid SPIONs were removed by washing, and MEFs were harvested by scraping in PBS. After centrifugation (200 *g*, 10 min), cell pellets were resuspended in 250 mM sucrose (supplemented with 10 mM Hepes; 1 mM EDTA, pH 7.4; and PIs; Roche) and homogenized using a ball bearing cell cracker (20 passages, clearance 10 mm; Isobiotec) to obtain a total cell lysate. After low-speed centrifugation (200 *g*, 10 min), the PNS was loaded on a LS column (equilibrated with PBS) placed inside a strong magnetic field (SuperMACSII; Miltenyi Biotec). Liquid separation columns are packed with a hydrophilically coated matrix that strongly enhances the magnetic field and thereby ensures a more efficient retention of amino lipid SPIONs (and adhering PMs) on the column. Within the magnetic field, the nonmagnetic fraction is first removed, followed by extensive and sequential washes with ice-cold homogenization buffer, high-salt 1 M KCl, and high-pH 0.1 M Na_2CO_3 buffers to maximally remove any unbound material. The PM fraction was eluted from the column by removal of the magnetic field. Next, the magnet was removed, and the bound fraction was eluted. Following high-speed ultracentrifugation (126,000 *g*, 1 h), the resulting pellet was resuspended in 200 µl homogenization buffer and subjected to further analysis. Equal amounts of total cell lysate and bound fractions were analyzed by SDS-PAGE and BN-PAGE, followed by Western blotting.

Cell surface biotinylation

Subconfluent cells were washed three times with Dulbecco's PBS (pH 8.0–8.5), followed by incubation (30 min, 4°C) in PBS containing 0.5 mg/ml Sulfo-NHS-SS-Biotin (Pierce). After washing with PBS, unbound biotin was quenched (15 min, 4°C) with PBS containing 100 mM glycine and 0.5% BSA and next washed with PBS containing 100 mM glycine. Cells were extracted in a salt buffer containing 1% Triton X-100 (100 mM NaCl; 50 mM Hepes, pH 7.2; 1% Triton X-100; PI) and extracts cleared (21,000 g_{avg}, 15 min). The protein concentration was determined, and equal amounts of extract (500 µg) were incubated overnight (4°C) with streptavidin Sepharose beads (GE Healthcare). Input and bound biotinylated proteins were processed for Western blotting.

In vitro translation

The procedure to translate and translocate newly synthesized proteins, in this case PSEN1, in the ER membrane of SICs (Kleizen et al., 2005; Wilson et al., 1995), followed by in vitro COPII-dependent budding, has been described previously (Kim et al., 2007). In brief, SICs were made from mouse Neuro2a cells to translate and translocate 35S-labeled PSEN1 into the ER membranes for 45 min at 30°C. To stop translation, we added 750 µl ice-cold KHM buffer (110 mM KOAc; 20 mM Hepes, pH 7.2; 2 mM MgOAc), and the SICs were harvested at 3,000 *g* for 3 min at 4°C, resuspended in ice-cold KHM, and used for budding reactions as described above. After incubating the budding reaction for 45 min at 30°C, differential centrifugation fractionated the SIC pellet at 12,000 *g* (input) and the vesicles from the supernatant at 100,000 *g*. To calculate the percentage of budding, we correlated the radiolabeled signal in the vesicle fractions (both −rATP and +rATP) to the radiolabeled signal in the ER pellet fractions of each translated protein. Nonspecific leakage found in the vesicle fractions from budding reactions −rATP were subtracted from radiolabeled signal found in vesicle fractions from budding reactions +rATP.

Coimmunoprecipitation

MEFs (from different genotypes) were grown to confluency, washed with ice-cold PBS (three times), and collected by scraping and centrifugation (2,000 g_{avg}, 5 min, 4°C). Cell pellets were resuspended in lysis buffer (50 mM Hepes, pH 7.4, 150 mM NaCl, 0.5% DDM, PI) and lysed for 1 h on ice. After centrifugation (20,000 g_{av}, 15 min, 4°C), the supernatant was collected, and the concentration was measured. For each sample, 200 µg protein was precleared by incubating with washed protein G Sepharose beads for 1 h at 4°C. Cleared lysate was incubated overnight at 4°C with 1 µl anti-NCT mAb (9C3; 1.33 µg/µl) under constant rotation. As negative controls, both protein extract without antibody and antibody without protein extract were used. After addition of 20 µl washed protein G Sepharose beads, the samples were incubated for 2 h at 4°C. Finally, the unbound fraction was collected, and beads were washed three times with ice-cold lysis buffer and once with TBS (5 mM Tris, 75 mM NaCl, pH 7.4). The proteins were denatured in 20 µl sample buffer and analyzed with SDS-PAGE. Total cell lysate (15 µg) was used as input, and unbound fraction (15 µg) from beads incubated with protein sample and antibody was used as unbound. Blots were probed with the following antibodies: mouse anti-NCT (9C3), rabbit anti-APH1A (B80.3), rabbit anti-PSEN1 NTF (B19.3), and rabbit anti–PEN-2 (ab18189; Abcam).

Gel electrophoresis and Western blotting

Western blotting

Protein concentrations were determined by Bio-Rad DC protein assay (Bio-Rad Laboratories). Samples were solubilized in NuPAGE sample buffer, separated by SDS-PAGE (4–12% Bis-Tris NuPAGE gels in MES running buffer; Life Technologies), and

transferred onto nitrocellulose membranes (Life Technologies). After blocking in 5% nonfat milk, membranes were incubated with primary antibody (4°C overnight) followed by washing and incubation with HRP-conjugated secondary antibodies (1 h, RT). After final washing, immunodetection was done using ECL (Western Lightning-Plus ECL; PerkinElmer), and immunoreactive protein bands were digitally captured and quantified on a Fuji MiniLAS 3000 imager (Fujifilm) using Aida Image Analyzer software (Raytest). Data are represented as mean ± SEM of at least three independent experiments. All statistical analyses were performed using Student's *t* test with significance levels as indicated on the figures.

BN-PAGE

Input membranes and COPII vesicles were resuspended (using a syringe and a 26-gauge needle) in fresh 25BTH20G buffer (20% glycerol; 25 mM Bis-Tris HCl; pH 7.0; 4°C) containing 0.5% DDM (Sigma-Aldrich) and PIs and solubilized for 1 h at 4°C. The extract was cleared by two ultracentrifugation steps for 30 min and 15 min at 126,200 g_{av} (4°C). Equal amounts of protein extract were mixed with 5× blue native sample buffer (2.5% Coomassie Brilliant Blue G-250 [Pierce]; 50 mM Bis-Tris HCl; 250 mM 6-aminocaproic acid, pH 7.0; 15% sucrose). BN-PAGE was performed at 4°C on 4–16% precast NativePAGE Novex Bis-Tris gel (Invitrogen). Molecular mass markers were prepared by resuspending a vial of HMW native marker kit (Amersham) in 75 µl 25BTH20G, 5 µl 10% DDM, and 20 µl 5× blue native sample buffer. Before transfer on Immobilon-P polyvinylidene fluoride membrane (EMD Millipore), gels were preincubated in NuPAGE transfer buffer (Invitrogen; 10 min, RT) containing 0.1% SDS and 20% methanol. Blots were destained for 1 h in destaining buffer (30% methanol, 10% acetic acid, 60% distilled H_2O) and further processed for Western blotting.

Cell-free γ-secretase assay

Membranes of subcellular fractions were obtained by ultracentrifugation, and the equivalent of 15 µg of membrane proteins was resuspended in 15 µl TE buffer (5 mM Tris-HCl, 1 mM EDTA, pH 7.0) containing 0.5% CHAPS and incubated for 1 h at 4°C. Extracts were incubated overnight at 37°C with 1 µl recombinant APP-C100-FLAG (Li et al., 2000), 1 µl DMSO, and 1 µl 1 M Tris-HCl, pH 7.0. De novo formed Aβ was analyzed by SDS-PAGE on a NuPAGE Novex 10% Bis-Tris gel (Life Technologies) in NuPAGE MES SDS running buffer, followed by Western blotting using mAb WO-2 and ECL detection.

CHX treatment

WT, NCT-KO, APH1-tKO, PSEN-dKO, and PEN-2-KO MEFs were grown in 6-cm dishes in DMEM/F-12 supplemented with 10% FBS until 90–100% confluency was reached and treated without and with 30 µg/ml CHX (Sigma-Aldrich). After 6 h and 24 h, cells were washed with ice-cold $PBS^{+/+}$ cells, harvested, and lysed in sucrose–Tris–EDTA buffer containing 1% Triton X-100. Equal amounts (20 µg) of cleared protein extract were analyzed by SDS-PAGE and Western blotting, as described.

Endoglycosidase H (endoH)/endoF treatment

Cells were grown in 6-cm dishes in DMEM/F-12 supplemented with 10% FBS until 90–100% confluency was reached. Cells were scraped and lysed in 1% Triton X-100 lysis buffer (150 mM NaCl, 50 mM Hepes, pH 7.4, 1% Triton X-100, PI). Protein concentrations were determined by Bio-Rad DC protein assay (Bio-Rad Laboratories), and 20 µg protein was treated with endoH or PNGaseF (all from New England Biolabs) or was left untreated according to the manufacturer's guidelines. Samples were processed for Western blotting as described previously.

Light microscopy and image analysis

Cells were fixed for 20 min at RT in 4% formaldehyde (Sigma-Aldrich) supplemented with 4% sucrose in 120 mM sodium phosphate buffer, pH 7.3, permeabilized for 5 min at RT with 0.1% Triton X-100, and blocked for 1 h at RT in blocking buffer (2% wt/vol BSA, 2% vol/vol FBS, 1% gelatin vol/vol, and 2% vol/vol goat serum in PBS). After 2-h incubation at RT with primary antibody diluted in blocking buffer, cells were incubated for 30 min at RT with secondary antibody diluted in blocking buffer and mounted using Mowiol (Sigma-Aldrich). Confocal imaging was performed on a Leica TCS SP5 II microscope (Leica Microsystems) connected to an upright microscope, using an oil-immersion plan apochromat 60×/1.40 NA objective lens. Image acquisition was performed with LAS software (Leica Microsystems). Super-resolution imaging was performed on an inverted Zeiss LSM880 microscope equipped with a fast Airyscan module (Carl Zeiss Microscopy), using an oil-immersion plan apochromat 60×/1.4 NA objective lens and controlled by ZEN black software (Carl Zeiss Microscopy). Images were further processed with Fiji (https://imagej.net/Fiji) and Photoshop CS6 (Adobe).

Online supplemental material

Fig. S1 A shows SDS-PAGE of in vitro COPII budding reactions from primary cortical mouse neurons and rat glia. Fig. S1, B–F, shows quality control of the different subcellular fractionation protocols. Fig. S2 contains Western blots as part of the quality control for stable expression of GFP-PSEN1 in PSEN-dKO MEFs. Fig. S3 A displays BN-PAGE of in vitro COPII budding reactions in primary rat glia. Fig. S3 B shows SDS-PAGE of NCT coimmunoprecipitation. Fig. S3, C–E, shows in vitro COPII budding reactions after in vitro translation of WT and mutant PSEN1. Fig. S3, F and G, presents quality control of cell lines expressing GFP-PSEN1-WT and GFP-PSEN1-APA stably transduced in PSEN-dKO MEFs. Fig. S4 shows characterization and in vitro COPII budding reactions of cell lines expressing NCT deletion mutants. Fig. S5 exhibits the effect of different detergents on the migration of γ-secretase (sub)complexes in BN-PAGE gels. Video 1 shows a rotating structural model of γ-secretase.

Acknowledgments

We thank P. Wong (Baltimore, MD) for NCT KO MEFs and B. De Strooper (Katholieke Universiteit Leuven, Leuven, Belgium) for other subunit KO MEFs.

This work was financed through Vlaams Instituut voor Biotechnologie, Katholieke Universiteit Leuven (C16/15/073, C14/21/095), Research Foundation–Flanders (S006617N, G078117N, G056017N, AKUL13/39), and Stichting Alzheimer Onderzoek–Alzheimer

Research Foundation (S#20030). R. Wouters held a Research Foundation–Flanders aspirant fellowship, and B. Kleizen held a long-term European Molecular Biology Organization fellowship. R. Schekman is supported as an investigator of the Howard Hughes Medical Institute and the Adolph C. and Mary Sprague Miller Institute for Basic Research in Science, University of California, Berkeley.

The authors declare no competing financial interests.

Author contributions: C. Michiels, R. Wouters, B. Kleizen, and R. Sannerud performed ER budding assays. R. Wouters and K. Dillen performed coimmunoprecipitation and cell fractionations. R. Sannerud, R. Wouters, and A. Escamilla Ayala performed imaging. D. Demedts performed PM isolations. W. Vermeire performed biochemical analysis. R. Wouters, R. Sannerud, B. Kleizen, R. Schekman, and W. Annaert coordinated the experiments and data interpretation. W. Annaert and R. Wouters designed and created figures. W. Annaert, B. Kleizen, and R. Wouters wrote the manuscript and harmonized the input of all other authors.

Submitted: 25 November 2019
Revised: 29 December 2020
Accepted: 7 June 2021

References

Adolf, F., M. Rhiel, I. Reckmann, and F.T. Wieland. 2016. Sec24C/D-isoform-specific sorting of the preassembled ER-Golgi Q-SNARE complex. *Mol. Biol. Cell.* 27:2697–2707. https://doi.org/10.1091/mbc.e16-04-0229

Adolf, F., M. Rhiel, B. Hessling, Q. Gao, A. Hellwig, J. Béthune, and F.T. Wieland. 2019. Proteomic profiling of mammalian COPII and COPI vesicles. *Cell Rep.* 26:250–265.e5. https://doi.org/10.1016/j.celrep.2018.12.041

Annaert, W., and C. Kaether. 2020. Bring it back, bring it back, don't take it away from me – the sorting receptor RER1. *J. Cell Sci.* 133:jcs231423. https://doi.org/10.1242/jcs.231423

Annaert, W.G., L. Levesque, K. Craessaerts, I. Dierinck, G. Snellings, D. Westaway, P.S. George-Hyslop, B. Cordell, P. Fraser, and B. De Strooper. 1999. Presenilin 1 controls γ-secretase processing of amyloid precursor protein in pre-Golgi compartments of hippocampal neurons. *J. Cell Biol.* 147:277–294. https://doi.org/10.1083/jcb.147.2.277

Bai, X.C., C. Yan, G. Yang, P. Lu, D. Ma, L. Sun, R. Zhou, S.H.W. Scheres, and Y. Shi. 2015. An atomic structure of human γ-secretase. *Nature.* 525:212–217. https://doi.org/10.1038/nature14892

Bammens, L., L. Chávez-Gutiérrez, A. Tolia, A. Zwijsen, and B. De Strooper. 2011. Functional and topological analysis of Pen-2, the fourth subunit of the γ-secretase complex. *J. Biol. Chem.* 286:12271–12282. https://doi.org/10.1074/jbc.M110.216978

Bancher, C., C. Brunner, H. Lassmann, H. Budka, K. Jellinger, G. Wiche, F. Seitelberger, I. Grundke-Iqbal, K. Iqbal, and H.M. Wisniewski. 1989. Accumulation of abnormally phosphorylated tau precedes the formation of neurofibrillary tangles in Alzheimer's disease. *Brain Res.* 477:90–99. https://doi.org/10.1016/0006-8993(89)91396-6

Banker, G., and K. Goslin. 1998. Culturing Nerve Cells. MIT Press, Cambridge, MA.

Barlowe, C., and R. Schekman. 1993. SEC12 encodes a guanine-nucleotide-exchange factor essential for transport vesicle budding from the ER. *Nature.* 365:347–349. https://doi.org/10.1038/365347a0

Barlowe, C., L. Orci, T. Yeung, M. Hosobuchi, S. Hamamoto, N. Salama, M.F. Rexach, M. Ravazzola, M. Amherdt, and R. Schekman. 1994. COPII: a membrane coat formed by Sec proteins that drive vesicle budding from the endoplasmic reticulum. *Cell.* 77:895–907. https://doi.org/10.1016/0092-8674(94)90138-4

Bickford, L.C., E. Mossessova, and J. Goldberg. 2004. A structural view of the COPII vesicle coat. *Curr. Opin. Struct. Biol.* 14:147–153. https://doi.org/10.1016/j.sbi.2004.02.002

Capell, A., D. Beher, S. Prokop, H. Steiner, C. Kaether, M.S. Shearman, and C. Haass. 2005. γ-Secretase complex assembly within the early secretory pathway. *J. Biol. Chem.* 280:6471–6478. https://doi.org/10.1074/jbc.M409106200

Chen, F., H. Hasegawa, G. Schmitt-Ulms, T. Kawarai, C. Bohm, T. Katayama, Y. Gu, N. Sanjo, M. Glista, E. Rogaeva, et al. 2006. TMP21 is a presenilin complex component that modulates γ-secretase but not ε-secretase activity. *Nature.* 440:1208–1212. https://doi.org/10.1038/nature04667

De Strooper, B. 2014. Lessons from a failed γ-secretase Alzheimer trial. *Cell.* 159:721–726. https://doi.org/10.1016/j.cell.2014.10.016

De Strooper, B., and W. Annaert. 2010. Novel research horizons for presenilins and γ-secretases in cell biology and disease. *Annu. Rev. Cell Dev. Biol.* 26:235–260. https://doi.org/10.1146/annurev-cellbio-100109-104117

De Strooper, B., P. Saftig, K. Craessaerts, H. Vanderstichele, G. Guhde, W. Annaert, K. Von Figura, and F. Van Leuven. 1998. Deficiency of presenilin-1 inhibits the normal cleavage of amyloid precursor protein. *Nature.* 391:387–390. https://doi.org/10.1038/34910

Dukhovny, A., A. Papadopulos, and K. Hirschberg. 2008. Quantitative live-cell analysis of microtubule-uncoupled cargo-protein sorting in the ER. *J. Cell Sci.* 121:865–876. https://doi.org/10.1242/jcs.019463

Edbauer, D., E. Winkler, J.T. Regula, B. Pesold, H. Steiner, and C. Haass. 2003. Reconstitution of γ-secretase activity. *Nat. Cell Biol.* 5:486–488. https://doi.org/10.1038/ncb960

Ellgaard, L., and A. Helenius. 2003. Quality control in the endoplasmic reticulum. *Nat. Rev. Mol. Cell Biol.* 4:181–191. https://doi.org/10.1038/nrm1052

Escamilla-Ayala, A., R. Wouters, R. Sannerud, and W. Annaert. 2020a. Contribution of the presenilins in the cell biology, structure and function of γ-secretase. *Semin. Cell Dev. Biol.* 105:12–26. https://doi.org/10.1016/j.semcdb.2020.02.005

Escamilla-Ayala, A.A., R. Sannerud, M. Mondin, K. Poersch, W. Vermeire, L. Paparelli, C. Berlage, M. Koenig, L. Chavez-Gutierrez, M.H. Ulbrich, et al. 2020b. Super-resolution microscopy reveals majorly mono- and dimeric presenilin1/γ-secretase at the cell surface. *eLife.* 9:e56679. https://doi.org/10.7554/eLife.56679

Esselens, C., V. Oorschot, V. Baert, T. Raemaekers, K. Spittaels, L. Serneels, H. Zheng, P. Saftig, B. De Strooper, J. Klumperman, et al. 2004. Presenilin 1 mediates the turnover of telencephalin in hippocampal neurons via an autophagic degradative pathway. *J. Cell Biol.* 166:1041–1054. https://doi.org/10.1083/jcb.200406060

Fath, S., J.D. Mancias, X. Bi, and J. Goldberg. 2007. Structure and organization of coat proteins in the COPII cage. *Cell.* 129:1325–1336. https://doi.org/10.1016/j.cell.2007.05.036

Fraering, P.C., M.J. LaVoie, W. Ye, B.L. Ostaszewski, W.T. Kimberly, D.J. Selkoe, and M.S. Wolfe. 2004a. Detergent-dependent dissociation of active γ-secretase reveals an interaction between Pen-2 and PS1-NTF and offers a model for subunit organization within the complex. *Biochemistry.* 43:323–333. https://doi.org/10.1021/bi035748j

Fraering, P.C., W. Ye, J.M. Strub, G. Dolios, M.J. LaVoie, B.L. Ostaszewski, A. van Dorsselaer, R. Wang, D.J. Selkoe, and M.S. Wolfe. 2004b. Purification and characterization of the human γ-secretase complex. *Biochemistry.* 43:9774–9789. https://doi.org/10.1021/bi0494976

Gomez-Navarro, N., A. Melero, X.H. Li, J. Boulanger, W. Kukulski, and E.A. Miller. 2020. Cargo crowding contributes to sorting stringency in COPII vesicles. *J. Cell Biol.* 219:e201806038. https://doi.org/10.1083/jcb.201806038

Gorvel, J.P., P. Chavrier, M. Zerial, and J. Gruenberg. 1991. rab5 controls early endosome fusion in vitro. *Cell.* 64:915–925. https://doi.org/10.1016/0092-8674(91)90316-Q

Haapasalo, A., and D.M. Kovacs. 2011. The many substrates of presenilin/γ-secretase. *J. Alzheimers Dis.* 25:3–28. https://doi.org/10.3233/JAD-2011-101065

Hammond, C., and A. Helenius. 1994. Quality control in the secretory pathway: retention of a misfolded viral membrane glycoprotein involves cycling between the ER, intermediate compartment, and Golgi apparatus. *J. Cell Biol.* 126:41–52. https://doi.org/10.1083/jcb.126.1.41

Hébert, S.S., L. Serneels, T. Dejaegere, K. Horré, M. Dabrowski, V. Baert, W. Annaert, D. Hartmann, and B. De Strooper. 2004. Coordinated and widespread expression of γ-secretase in vivo: evidence for size and molecular heterogeneity. *Neurobiol. Dis.* 17:260–272. https://doi.org/10.1016/j.nbd.2004.08.002

Holmes, O., S. Paturi, D.J. Selkoe, and M.S. Wolfe. 2014. Pen-2 is essential for γ-secretase complex stability and trafficking but partially dispensable for endoproteolysis. *Biochemistry.* 53:4393–4406. https://doi.org/10.1021/bi500489j

Iwatsubo, T., A. Odaka, N. Suzuki, H. Mizusawa, N. Nukina, and Y. Ihara. 1994. Visualization of Aβ42(43) and Aβ40 in senile plaques with end-

specific Aβ monoclonals: evidence that an initially deposited species is Aβ42(43). *Neuron.* 13:45–53. https://doi.org/10.1016/0896-6273(94)90458-8

Jarrett, J.T., E.P. Berger, and P.T. Lansbury Jr. 1993. The carboxy terminus of the beta amyloid protein is critical for the seeding of amyloid formation: implications for the pathogenesis of Alzheimer's disease. *Biochemistry.* 32:4693–4697. https://doi.org/10.1021/bi00069a001

Jurisch-Yaksi, N., R. Sannerud, and W. Annaert. 2013. A fast growing spectrum of biological functions of γ-secretase in development and disease. *Biochim. Biophys. Acta.* 1828:2815–2827. https://doi.org/10.1016/j.bbamem.2013.04.016

Kaether, C., J. Scheuermann, M. Fassler, S. Zilow, K. Shirotani, C. Valkova, B. Novak, S. Kacmar, H. Steiner, and C. Haass. 2007. Endoplasmic reticulum retention of the γ-secretase complex component Pen2 by Rer1. *EMBO Rep.* 8:743–748. https://doi.org/10.1038/sj.embor.7401027

Kim, S.H., Y.I. Yin, Y.M. Li, and S.S. Sisodia. 2004. Evidence that assembly of an active γ-secretase complex occurs in the early compartments of the secretory pathway. *J. Biol. Chem.* 279:48615–48619. https://doi.org/10.1074/jbc.C400396200

Kim, J., S. Hamamoto, M. Ravazzola, L. Orci, and R. Schekman. 2005. Uncoupled packaging of amyloid precursor protein and presenilin 1 into coat protein complex II vesicles. *J. Biol. Chem.* 280:7758–7768. https://doi.org/10.1074/jbc.M411091200

Kim, J., B. Kleizen, R. Choy, G. Thinakaran, S.S. Sisodia, and R.W. Schekman. 2007. Biogenesis of γ-secretase early in the secretory pathway. *J. Cell Biol.* 179:951–963. https://doi.org/10.1083/jcb.200709012

Kimberly, W.T., M.J. LaVoie, B.L. Ostaszewski, W. Ye, M.S. Wolfe, and D.J. Selkoe. 2003. γ-Secretase is a membrane protein complex comprised of presenilin, nicastrin, Aph-1, and Pen-2. *Proc. Natl. Acad. Sci. USA.* 100:6382–6387. https://doi.org/10.1073/pnas.1037392100

Kleizen, B., T. van Vlijmen, H.R. de Jonge, and I. Braakman. 2005. Folding of CFTR is predominantly cotranslational. *Mol. Cell.* 20:277–287. https://doi.org/10.1016/j.molcel.2005.09.007

LaVoie, M.J., P.C. Fraering, B.L. Ostaszewski, W. Ye, W.T. Kimberly, M.S. Wolfe, and D.J. Selkoe. 2003. Assembly of the γ-secretase complex involves early formation of an intermediate subcomplex of Aph-1 and nicastrin. *J. Biol. Chem.* 278:37213–37222. https://doi.org/10.1074/jbc.M303941200

Lee, M.C., E.A. Miller, J. Goldberg, L. Orci, and R. Schekman. 2004. Bi-directional protein transport between the ER and Golgi. *Annu. Rev. Cell Dev. Biol.* 20:87–123. https://doi.org/10.1146/annurev.cellbio.20.010403.105307

Li, Y.M., M.T. Lai, M. Xu, Q. Huang, J. DiMuzio-Mower, M.K. Sardana, X.P. Shi, K.C. Yin, J.A. Shafer, and S.J. Gardell. 2000. Presenilin 1 is linked with γ-secretase activity in the detergent solubilized state. *Proc. Natl. Acad. Sci. USA.* 97:6138–6143. https://doi.org/10.1073/pnas.110126897

Li, T., G. Ma, H. Cai, D.L. Price, and P.C. Wong. 2003. Nicastrin is required for assembly of presenilin/γ-secretase complexes to mediate Notch signaling and for processing and trafficking of beta-amyloid precursor protein in mammals. *J. Neurosci.* 23:3272–3277. https://doi.org/10.1523/JNEUROSCI.23-08-03272.2003

Mancias, J.D., and J. Goldberg. 2007. The transport signal on Sec22 for packaging into COPII-coated vesicles is a conformational epitope. *Mol. Cell.* 26:403–414. https://doi.org/10.1016/j.molcel.2007.03.017

Mancias, J.D., and J. Goldberg. 2008. Structural basis of cargo membrane protein discrimination by the human COPII coat machinery. *EMBO J.* 27:2918–2928. https://doi.org/10.1038/emboj.2008.208

Margeta-Mitrovic, M., Y.N. Jan, and L.Y. Jan. 2000. A trafficking checkpoint controls $GABA_B$ receptor heterodimerization. *Neuron.* 27:97–106. https://doi.org/10.1016/S0896-6273(00)00012-X

McCaughey, J., and D.J. Stephens. 2019. ER-to-Golgi transport: a sizeable problem. *Trends Cell Biol.* 29:940–953. https://doi.org/10.1016/j.tcb.2019.08.007

Michelsen, K., H. Yuan, and B. Schwappach. 2005. Hide and run. Arginine-based endoplasmic-reticulum-sorting motifs in the assembly of heteromultimeric membrane proteins. *EMBO Rep.* 6:717–722. https://doi.org/10.1038/sj.embor.7400480

Miller, E., B. Antonny, S. Hamamoto, and R. Schekman. 2002. Cargo selection into COPII vesicles is driven by the Sec24p subunit. *EMBO J.* 21:6105–6113. https://doi.org/10.1093/emboj/cdf605

Miller, E.A., T.H. Beilharz, P.N. Malkus, M.C. Lee, S. Hamamoto, L. Orci, and R. Schekman. 2003. Multiple cargo binding sites on the COPII subunit Sec24p ensure capture of diverse membrane proteins into transport vesicles. *Cell.* 114:497–509. https://doi.org/10.1016/S0092-8674(03)00609-3

Miller, E.A., Y. Liu, C. Barlowe, and R. Schekman. 2005. ER-Golgi transport defects are associated with mutations in the Sed5p-binding domain of the COPII coat subunit, Sec24p. *Mol. Biol. Cell.* 16:3719–3726. https://doi.org/10.1091/mbc.e05-03-0262

Mossessova, E., L.C. Bickford, and J. Goldberg. 2003. SNARE selectivity of the COPII coat. *Cell.* 114:483–495. https://doi.org/10.1016/S0092-8674(03)00608-1

Nishimura, N., S. Bannykh, S. Slabough, J. Matteson, Y. Altschuler, K. Hahn, and W.E. Balch. 1999. A di-acidic (DXE) code directs concentration of cargo during export from the endoplasmic reticulum. *J. Biol. Chem.* 274:15937–15946. https://doi.org/10.1074/jbc.274.22.15937

Nohturfft, A., D. Yabe, J.L. Goldstein, M.S. Brown, and P.J. Espenshade. 2000. Regulated step in cholesterol feedback localized to budding of SCAP from ER membranes. *Cell.* 102:315–323. https://doi.org/10.1016/S0092-8674(00)00037-4

Nyabi, O., M. Bentahir, K. Horré, A. Herreman, N. Gottardi-Littell, C. Van Broeckhoven, P. Merchiers, K. Spittaels, W. Annaert, and B. De Strooper. 2003. Presenilins mutated at Asp-257 or Asp-385 restore Pen-2 expression and nicastrin glycosylation but remain catalytically inactive in the absence of wild type presenilin. *J. Biol. Chem.* 278:43430–43436. https://doi.org/10.1074/jbc.M306957200

Park, H.J., D. Shabashvili, M.D. Nekorchuk, E. Shyqyriu, J.I. Jung, T.B. Ladd, B.D. Moore, K.M. Felsenstein, T.E. Golde, and S.H. Kim. 2012. Retention in endoplasmic reticulum 1 (RER1) modulates amyloid-β (Aβ) production by altering trafficking of γ-secretase and amyloid precursor protein (APP). *J. Biol. Chem.* 287:40629–40640. https://doi.org/10.1074/jbc.M112.418442

Petit, D., M. Hitzenberger, S. Lismont, K.M. Zoltowska, N.S. Ryan, M. Mercken, F. Bischoff, M. Zacharias, and L. Chávez-Gutiérrez. 2019. Extracellular interface between APP and nicastrin regulates Aβ length and response to γ-secretase modulators. *EMBO J.* 38:e101494. https://doi.org/10.15252/embj.2019101494

Pettersen, E.F., T.D. Goddard, C.C. Huang, G.S. Couch, D.M. Greenblatt, E.C. Meng, and T.E. Ferrin. 2004. UCSF Chimera—a visualization system for exploratory research and analysis. *J. Comput. Chem.* 25:1605–1612. https://doi.org/10.1002/jcc.20084

Prokop, S., K. Shirotani, D. Edbauer, C. Haass, and H. Steiner. 2004. Requirement of PEN-2 for stabilization of the presenilin N-/C-terminal fragment heterodimer within the γ-secretase complex. *J. Biol. Chem.* 279:23255–23261. https://doi.org/10.1074/jbc.M401789200

Sannerud, R., and W. Annaert. 2009. Trafficking, a key player in regulated intramembrane proteolysis. *Semin. Cell Dev. Biol.* 20(2):183–190. https://doi.org/10.1016/j.semcdb.2008.11.004

Sannerud, R., C. Esselens, P. Ejsmont, R. Mattera, L. Rochin, A.K. Tharkeshwar, G. De Baets, V. De Wever, R. Habets, V. Baert, et al. 2016. Restricted location of PSEN2/γ-secretase determines substrate specificity and generates an intracellular Aβ pool. *Cell.* 166:193–208. https://doi.org/10.1016/j.cell.2016.05.020

Sato, M., K. Sato, and A. Nakano. 1996. Endoplasmic reticulum localization of Sec12p is achieved by two mechanisms: Rer1p-dependent retrieval that requires the transmembrane domain and Rer1p-independent retention that involves the cytoplasmic domain. *J. Cell Biol.* 134:279–293. https://doi.org/10.1083/jcb.134.2.279

Schweizer, A., K. Matter, C.M. Ketcham, and H.P. Hauri. 1991. The isolated ER-Golgi intermediate compartment exhibits properties that are different from ER and cis-Golgi. *J. Cell Biol.* 113:45–54. https://doi.org/10.1083/jcb.113.1.45

Scott, D.B., T.A. Blanpied, and M.D. Ehlers. 2003. Coordinated PKA and PKC phosphorylation suppresses RXR-mediated ER retention and regulates the surface delivery of NMDA receptors. *Neuropharmacology.* 45:755–767. https://doi.org/10.1016/S0028-3908(03)00250-8

Selkoe, D.J., and J. Hardy. 2016. The amyloid hypothesis of Alzheimer's disease at 25 years. *EMBO Mol. Med.* 8:595–608. https://doi.org/10.15252/emmm.201606210

Serneels, L., T. Dejaegere, K. Craessaerts, K. Horré, E. Jorissen, T. Tousseyn, S. Hébert, M. Coolen, G. Martens, A. Zwijsen, et al. 2005. Differential contribution of the three Aph1 genes to γ-secretase activity in vivo. *Proc. Natl. Acad. Sci. USA.* 102:1719–1724. https://doi.org/10.1073/pnas.0408901102

Shimoni, Y., T. Kurihara, M. Ravazzola, M. Amherdt, L. Orci, and R. Schekman. 2000. Lst1p and Sec24p cooperate in sorting of the plasma membrane ATPase into COPII vesicles in *Saccharomyces cerevisiae*. *J. Cell Biol.* 151:973–984. https://doi.org/10.1083/jcb.151.5.973

Shirotani, K., D. Edbauer, S. Prokop, C. Haass, and H. Steiner. 2004. Identification of distinct γ-secretase complexes with different APH-1 variants. *J. Biol. Chem.* 279:41340–41345. https://doi.org/10.1074/jbc.M405768200

Spasic, D., and W. Annaert. 2008. Building γ-secretase: the bits and pieces. *J. Cell Sci.* 121:413–420. https://doi.org/10.1242/jcs.015255

Spasic, D., T. Raemaekers, K. Dillen, I. Declerck, V. Baert, L. Serneels, J. Füllekrug, and W. Annaert. 2007. Rer1p competes with APH-1 for

binding to nicastrin and regulates γ-secretase complex assembly in the early secretory pathway. *J. Cell Biol.* 176:629–640. https://doi.org/10.1083/jcb.200609180

Szaruga, M., B. Munteanu, S. Lismont, S. Veugelen, K. Horré, M. Mercken, T.C. Saido, N.S. Ryan, T. De Vos, S.N. Savvides, et al. 2017. Alzheimer's-causing mutations shift Aβ length by destabilizing γ-secretase-Aβn interactions. *Cell.* 170:443–456.e14. https://doi.org/10.1016/j.cell.2017.07.004

Takasugi, N., T. Tomita, I. Hayashi, M. Tsuruoka, M. Niimura, Y. Takahashi, G. Thinakaran, and T. Iwatsubo. 2003. The role of presenilin cofactors in the γ-secretase complex. *Nature.* 422:438–441. https://doi.org/10.1038/nature01506

Tharkeshwar, A.K., J. Trekker, W. Vermeire, J. Pauwels, R. Sannerud, D.A. Priestman, D. Te Vruchte, K. Vints, P. Baatsen, J.P. Decuypere, et al. 2017. A novel approach to analyze lysosomal dysfunctions through subcellular proteomics and lipidomics: the case of NPC1 deficiency. *Sci. Rep.* 7:41408. https://doi.org/10.1038/srep41408

Thimiri Govinda Raj, D.B., B. Ghesquière, A.K. Tharkeshwar, K. Coen, R. Derua, D. Vanderschaeghe, E. Rysman, M. Bagadi, P. Baatsen, B. De Strooper, et al. 2011. A novel strategy for the comprehensive analysis of the biomolecular composition of isolated plasma membranes. *Mol. Syst. Biol.* 7:541. https://doi.org/10.1038/msb.2011.74

Wakabayashi, T., K. Craessaerts, L. Bammens, M. Bentahir, F. Borgions, P. Herdewijn, A. Staes, E. Timmerman, J. Vandekerckhove, E. Rubinstein, et al. 2009. Analysis of the γ-secretase interactome and validation of its association with tetraspanin-enriched microdomains. *Nat. Cell Biol.* 11:1340–1346. https://doi.org/10.1038/ncb1978

Wilson, R., A.J. Allen, J. Oliver, J.L. Brookman, S. High, and N.J. Bulleid. 1995. The translocation, folding, assembly and redox-dependent degradation of secretory and membrane proteins in semi-permeabilized mammalian cells. *Biochem. J.* 307:679–687. https://doi.org/10.1042/bj3070679

Wolfe, M.S., W. Xia, B.L. Ostaszewski, T.S. Diehl, W.T. Kimberly, and D.J. Selkoe. 1999. Two transmembrane aspartates in presenilin-1 required for presenilin endoproteolysis and γ-secretase activity. *Nature.* 398:513–517. https://doi.org/10.1038/19077

Xia, H., Z.D. Hornby, and R.C. Malenka. 2001. An ER retention signal explains differences in surface expression of NMDA and AMPA receptor subunits. *Neuropharmacology.* 41:714–723. https://doi.org/10.1016/S0028-3908(01)00103-4

Yang, G., R. Zhou, X. Guo, C. Yan, J. Lei, and Y. Shi. 2021. Structural basis of γ-secretase inhibition and modulation by small molecule drugs. *Cell.* 184:521–533.e14. https://doi.org/10.1016/j.cell.2020.11.049

Zanetti, G., K.B. Pahuja, S. Studer, S. Shim, and R. Schekman. 2012. COPII and the regulation of protein sorting in mammals. *Nat. Cell Biol.* 14:20–28. https://doi.org/10.1038/ncb2390

Zerangue, N., B. Schwappach, Y.N. Jan, and L.Y. Jan. 1999. A new ER trafficking signal regulates the subunit stoichiometry of plasma membrane K(ATP) channels. *Neuron.* 22:537–548. https://doi.org/10.1016/S0896-6273(00)80708-4

Zhou, S., H. Zhou, P.J. Walian, and B.K. Jap. 2005. CD147 is a regulatory subunit of the γ-secretase complex in Alzheimer's disease amyloid beta-peptide production. *Proc. Natl. Acad. Sci. USA.* 102:7499–7504. https://doi.org/10.1073/pnas.0502768102

JCB

Supplemental material

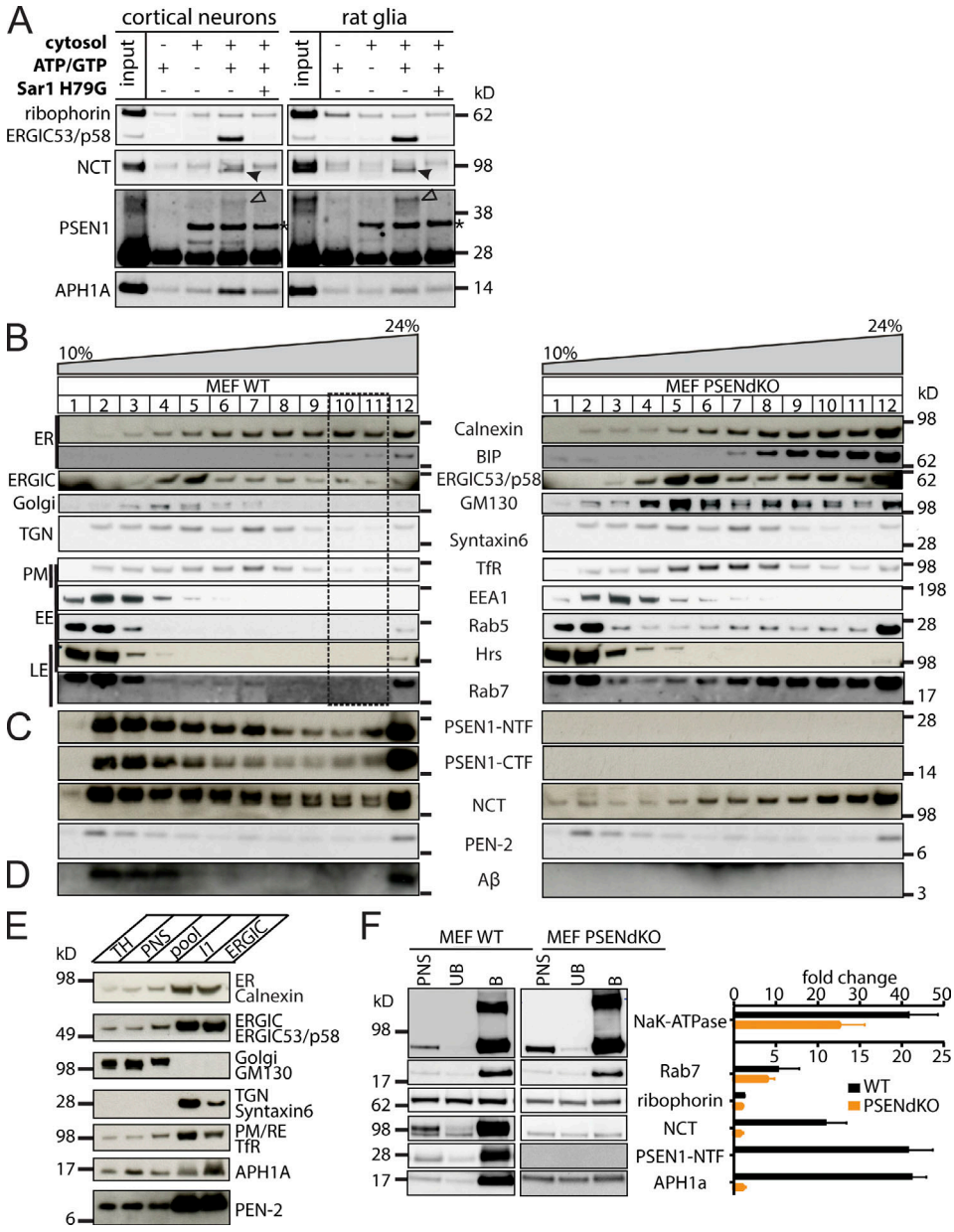

Figure S1. **In vitro ER budding in SICs derived from murine primary neurons and rat primary glial cells and isolation of secretory pathway compartments. (A)** SDS-PAGE and Western blot analysis of in vitro generated COPII vesicles from murine primary cortical neurons (7 d in vitro) and rat glial SICs: 4.2% of SICs (input) and 100% of COPII-coated vesicles were analyzed with the indicated antibodies. Reactions without nucleotides were used as a negative control. COPII budding was specifically inhibited by the GTP-restricted mutant Sar1b H79G. A representative Western blot shows COPII-dependent budding of immature NCT, FL PSEN1, and APH1A in both murine cortical neurons and rat glia (filled arrowheads: immature NCT; open arrowheads: FL PSEN1; asterisk: aspecific band). **(B–D)** Enrichment of the ER. Fractionation of MEF WT and MEF PSEN-dKO using a continuous 10–24% Nycodenz gradient followed by Western blotting (equal fraction volume per lane) for (B) ribophorin, calnexin, KDEL: ER; ERGIC53/p58: ERGIC; GM130: cis-Golgi; syntaxin 6: trans-Golgi Network (TGN); TfR: PM and recycling endosomes; EEA1, Rab5, Hrs: early endosomes (EE); Rab7: late endosomes (LE); (C) γ-secretase components; and (D) γ-secretase activity (after a cell-free γ-secretase assay). ER proteins are most strongly enriched in fractions 10 and 11, which were pooled as "enriched ER" for BN-PAGE. In WT cells, mature γ-secretase complex members (indicated by mature glycosylated NCT and PSEN1-NTF and –CTF) and de novo Aβ production, representing γ-secretase activity, comigrate only in fractions enriched for endosomal markers. In PSEN-deficient cells, immature NCT and PEN-2 are largely located to ER fractions. **(E)** γ-Secretase complex members are enriched in the ERGIC. Purification of the ERGIC combining Percoll gradient and discontinuous Nycodenz gradient centrifugation (see Materials and methods for details). The second step was needed to further separate the ERGIC from the trans-Golgi network (TGN), as shown by the comparative Western blot analysis of TH and PNS with the 18.5–27% interface of the Percoll gradient (I1) and final enriched ERGIC (equal amount of protein per lane). The ERGIC fraction is also devoid of the cis-Golgi marker GM130 but still contaminated with ER (calnexin). γ-Secretase complex members NCT, APH1, and PEN-2 coenrich with ERGIC-53/p58 with a stronger relative enrichment of immature NCT as expected from early biosynthetic compartments. **(F)** Magnetic isolation of PM from WT and PSEN-dKO MEFs using SPIONs. A representative Western blot showing PNS (postnuclear supernatant), UB (unbound fraction), and B (bound fraction) with quantification (n = 4 independent isolations) show strong enrichment for the PM marker, Na^+K^+-ATPase, along with PSEN1 and mature NCT, whereas the ER marker, ribophorin, does not enrich and the late endosomal Rab7 enriches only moderately, as described (Thimiri Govinda Raj et al., 2011).

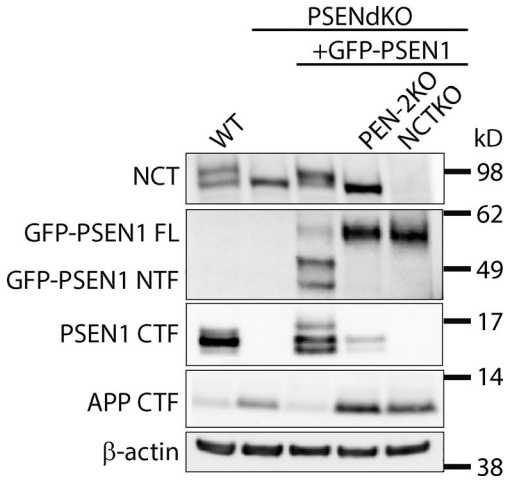

Figure S2. **Western blot of cell lines stably expressing GFP-PSEN1.**

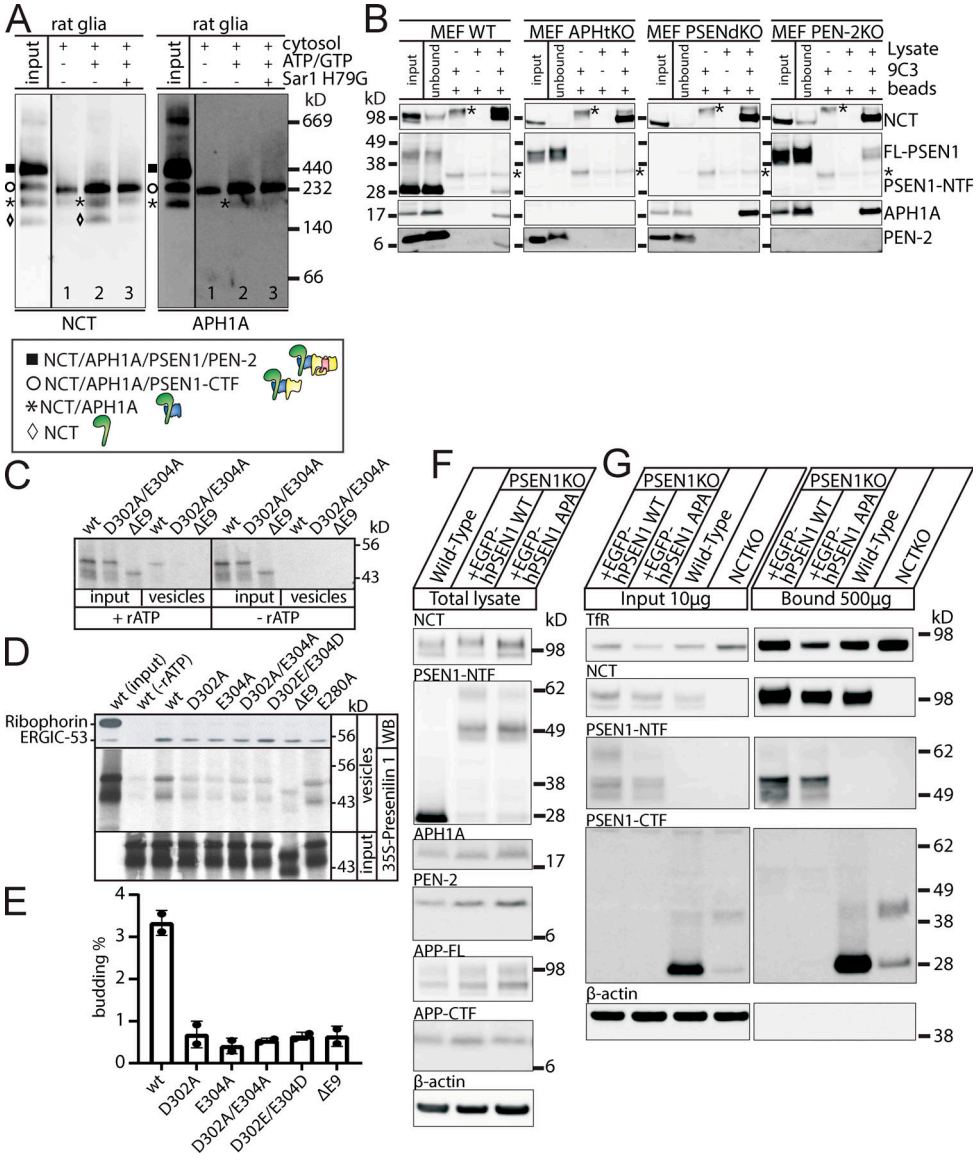

Figure S3. **Subcomplexes identified by BN-PAGE are confirmed in rat glia and by coimmunoprecipitation; the DXE motif in exon 9 is crucial for COPII-dependent export of PSEN1 from ER. (A)** BN-PAGE and Western blot analysis of γ-secretase in COPII vesicles generated from rat glial SICs. Monomeric NCT and dimeric NCT/APH1A show COPII-dependent budding. **(B)** A representative Western blot is shown comparing total cell extracts of WT, APH1-tKO, PSEN-dKO, and PEN-2-KO MEFs with the respective unbound and coimmunoprecipitated (using anti-NCT mAb 9C3, bound) fractions. For each cell line, omission of either 9C3 or extract was used as a negative control. Whereas 9C3 coimmunoprecipitates all subunits in WT extracts, only immature NCT was pulled down in APH1A-tKO extracts, and both immature NCT and APH1A were pulled down in PSEN-dKO extracts. In PEN-2-KO extracts, immature NCT, APH1A, and FL PSEN1 coimmunoprecipitated. These interactions are reminiscent of the subcomplexes identified by BN-PAGE. Note that APH1A is increasingly more present in the immunoprecipitates of PSEN-dKO and PEN-2-KO, respectively, and compared with WT extracts, confirming the accumulation of corresponding subcomplexes. Asterisk indicates an unrelated band also present in control lanes. **(C)** WT human PSEN1, the DPE mutant (D302A/D304A), and PSEN1ΔE9 were in vitro translated in SICs followed by the in vitro budding assay in the absence or presence of ATP. Radiolabeled PSEN1 variants from the pellet (SIC input) and vesicle fractions were compared on 10% SDS-PAGE gel. **(D)** WT human PSEN1 and PSEN1 mutants (DPE and ΔE9) were stably transfected, and next, SICs were made to determine the ER export efficiency of these PSEN1 variants at steady state. To better understand the DPE consensus site molecularly, we made subtler mutations, including the reversal of the two acidic amino acids followed by the analysis in C. Any manipulation of the DPE motifs dramatically impaired the ER export. WB, Western blot. **(E)** Quantification of the radiolabeled PSEN1 retrieved from the vesicle fractions that budded from the SICs (mean ± SD, n = 3). **(F)** PSEN-dKO were stably transduced with lentiviral vectors expressing either eGFP-tagged hPSEN1 or a mutant variant wherein the DPE motif in the cytosolic loop domain is altered to APA (eGFP-hPSEN1 APA) using site-directed mutagenesis. Western blot analysis shows that eGFP-hPSEN1 and –PSEN1 APA are equally expressed and accessible to endoproteolysis. In addition, mature glycosylation of NCT and PEN-2 stability are restored, whereas APP-CTF levels, the direct substrate for PSEN1, are not different, indicating that the APA mutation does not affect γ-secretase complex formation and activity. **(G)** Cell surface biotinylation of eGFP-hPSEN1 and –hPSEN1 APA compared with WT and NCT-KO MEFs shows no defect in the trafficking of the APA mutant to the cell surface. Input lanes represent 10 µg of protein; bound fractions are recovered from 500 µg total cell lysate using streptavidin pull-down assays. Equal amounts of PSEN1-NTF (using an anti-hPSEN1–specific antibody) as well as mature NCT are recovered in the bound fraction. A murine specific antibody was used to detect endogenous mPSEN1-CTF in WT and NCT-KO cells. Note that in NCT-KO MEFs, endoproteolysis of mPSEN1 is inhibited and some FL mPSEN1 (asterisk) reaches the cell surface. TfR and actin are used as positive and negative controls, respectively.

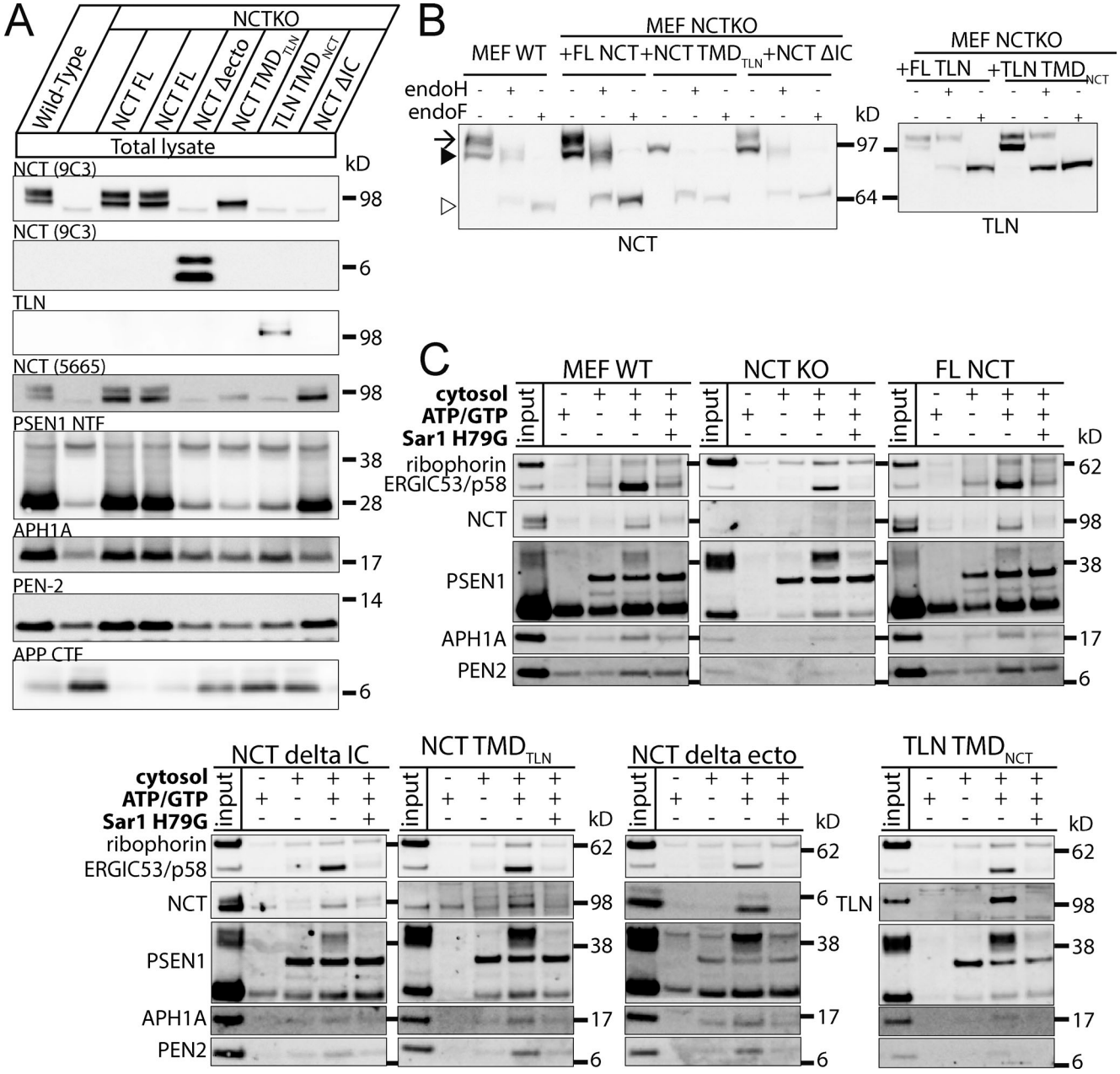

Figure S4. **NCT does not harbor a region/motif required for cargo sorting into COPII vesicles. (A)** NCT-KO cells were stably transduced with retroviral particles expressing FL NCT, deletion forms of NCT (Δecto: missing the ectodomain; ΔIC: missing the intracellular domain), NCT with a swapped TMD from TLN (NCT TMD_{TLN}), or TLN with the TMD of NCT (TLN TMD_{NCT}). Western blot analysis shows expression of all constructs, but only FL NCT and NCTΔIC rescue γ-secretase function, as monitored by a drop in APP CTF accumulation. **(B)** All cell lines described in A, except for NCT Δecto, were tested for glycosylation of NCT or TLN by endoH and endoF treatment (arrow: untreated; black arrowhead: endoH resistent; open arrowhead: endoH/F sensitive). For TLN TMD_{NCT}, FL TLN was expressed as a control for glycosylation. Although FL NCT and NCTΔIC expressed in NCT-KO cells are similarly glycosylated as NCT in WT cells, NCT TMD_{TLN} glycosylation failed to mature. TLN TMD_{NCT} glycosylation was similar to WT TLN. **(C)** SDS-PAGE and Western blot analysis of in vitro generated COPII vesicles from SICs of cell lines described in A: 4.2% of SICs (input) and 100% of COPII-coated vesicles were analyzed with the indicated antibodies. Reactions without nucleotides (ATP + GTP) or cytosol were used for background subtraction. COPII budding is specifically inhibited by the GTP-restricted mutant Sar1b H79G. Representative Western blot analysis of the COPII packaging using antibodies detecting ERGIC53/p58 as a positive control compared with antibodies against the different γ-secretase members. Antibodies to ribophorin were used as a negative control. In all cell lines, the different immature NCT variants or TLN and PSEN1 FL exited the ER in an Sar1-dependent manner.

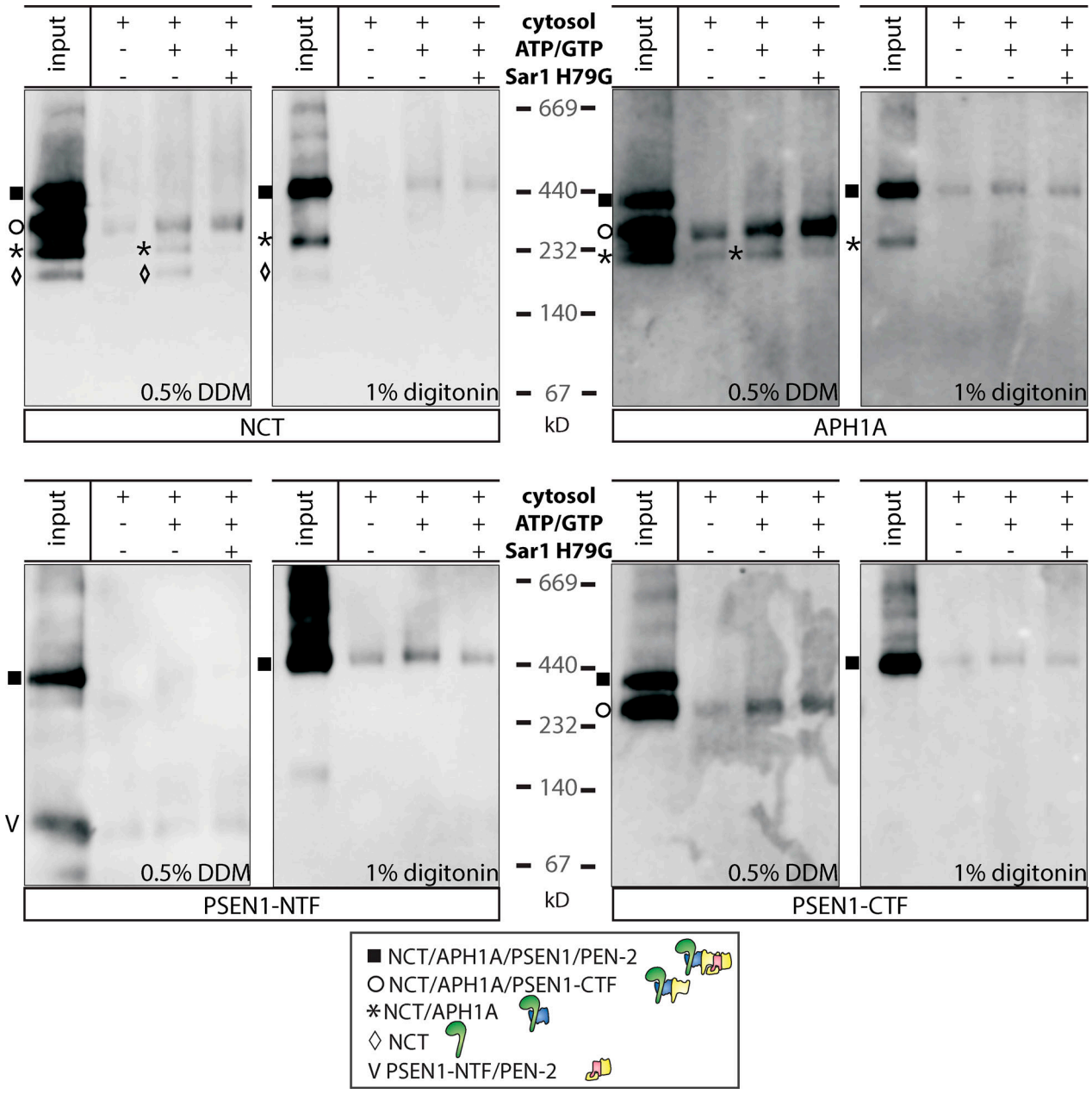

Figure S5. **Comparison of DDM and digitonin extraction for BN-PAGE analysis of COPII vesicles.** ER budding in WT SICs and analysis of γ-secretase complexes extracted by either 0.5% DDM or 1% digitonin using BN-PAGE followed by Western blotting for anti-NCT, -APH1A, and -PSEN1 fragments. In the case of DDM-extracted samples, both full complexes and subcomplexes and dimeric complexes were distinguished. Only monomeric NCT and dimeric NCT/APH1A subcomplexes exit the ER in an Sar1-dependent manner. In the case of 1% digitonin, essentially only full complexes were detected, but they lack Sar1 dependency in ER budding.

Video 1. **Rotating molecular structure.Rotating 360° lateral view of the 3D structure of γ-secretase generated using Chimera; with NCT (green), APH1A (blue), PSEN1 (orange), and PEN-2 (pink). Playback speed is 25 frames per second.**